Stony Brook University

An Investigation into the Effects of Process Parameters on the Quality of Laminates

A Thesis Presented

by

Haomin Liu

to

The Graduate School

in Partial Fulfillment of the

Requirements

for the Degree of

Master of Science

in

Materials Science and Engineering

Stony Brook University

May 2016

Stony Brook University

The Graduate School

Haomin Liu

We, the thesis committee for the above candidate for the

Master of Science degree, hereby recommend

acceptance of this thesis.

Qing Chang – Thesis Advisor

Assistant Professor, Mechanical Engineering

T Venkatesh – Committee member

Associate Professor and Graduate Program Director, Materials Science and Engineering

Balaji Raghothamachar – Committee member

Research Assistant Professor, Materials Science and Engineering

This thesis is accepted by the Graduate School

Charles Taber

Dean of the Graduate School

Abstract of the Thesis

An Investigation into the Effects of Process Parameters on the Quality of Laminates

by

Haomin Liu

Master of Science

in

Materials Science and Engineering

Stony Brook University

2016

In this work curing process for glass fiber reinforced polymer composite laminates is studied. Curing temperature, time and pressure were selected as the cure parameters for optimization. Central composite design (CCD) of design of experiment (DOE) approach was adopted for conducting the experiments. Flexural strength and flexural modulus of the composite laminate were the response measures to select the final cure parameters. Analysis of variance (ANOVA), surface plots and contour plots clearly demonstrate that temperature, time and pressure contribute greatly to the response functions. This establishes two models that can be used to predict the mechanical properties of composite laminated under certain manufactory parameters. Optimized solution is obtained under 300°F, 60 min, 321.717 psi.

Key Words: **Glass fiber reinforced polymer composite, Central composite design, Flexural strength, Flexural modulus**

Table of Contents

List of Figures

List of Tables

Chapter 1 Introduction

1.1 Motivation

The traditional manual layup of composite manufacturing is slowly being replaced by the automated layup in the modern field of aerospace, marine, automotive, and renewable energy. This is driven by the need for higher production efficiency and better manufacturing quality. To meet the increasing demand for high quality composites materials, two main automated processes for prepreg layup are used in composite products manufacturing, which are Automated Tape Laying (ATL) and Automated Fiber Placement (AFP). However, due to a variety of reasons related to productivity, reliability and price, these automated processes have the disadvantages of highly specialized and tailored for specific products, not minimize secondary debulking operations, and extremely expensive. Hence, the objective of this project is to advance the fundamental understanding of the relationship among composite materials properties, principal composite manufacturing processes (including processes relevant to automation) and fabricated products mechanical properties in order to enable high quality and high volume production and provide economic solutions that can fit the needs of composite manufactures.

1.2 Definition and Characteristics

A composite material is a material system consisting of two or more phases. Its mechanical performance and properties are designed to be superior to those of the independent materials. Usually one of the phases is discontinuous, stiffer, and stronger and is called the reinforcement, however the less stiff and weaker phase is continuous and is called the matrix. Sometimes, an

additional phase exists between the reinforcement and the matrix due to chemical interactions or processing effects and is called an interphase [1]. The phases of composite material are shown in Fig. 1.1 [2].

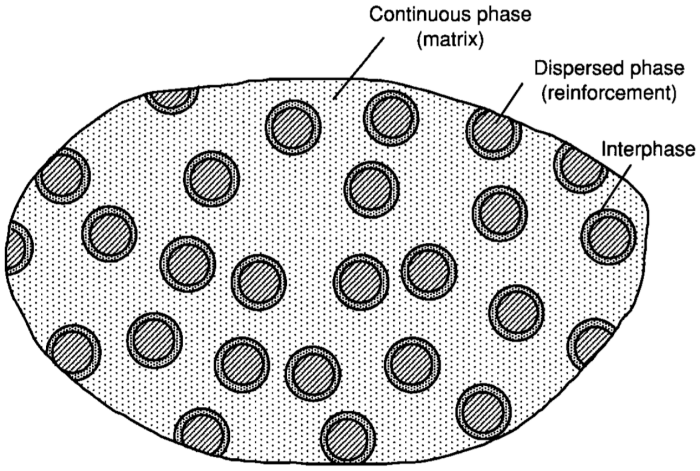

Fig. 1. 1 Phases of a composite material

The phases of the composite system play different roles. Take low- to medium-performance composite materials as an example, the reinforcement that is usually in the form of short fibers or particles may provide some stiffening but only limited strengthening of the material. The matrix, on the other hand, is the main load-bearing phase governing the mechanical properties of the material. The interphase, although small in dimensions, can play an important role in controlling the failure mechanisms, failure propagation, fracture toughness and the overall stress-strain behavior to failure of the material [2].

The properties of composite depend on three aspects: properties of the phases, geometry of dispersed phase including particle size, distribution and orientation, and the amount of phase. The fiber volume ratio is one of the most important parameters. The distribution of the reinforcement determines the homogeneity of the material. The more uniformly the

reinforcement distributes, the more homogeneous the material, and the lower the scatter in properties and the probability of failure in the weakest areas [3].

1.3 Historical Development and Applications

Composite materials are used in a wide variety of markets, including aerospace, architecture, automotive, energy, infrastructure, marine, military, and sports and recreation. The first uses of composites date back to the 1500s B.C. when early Egyptians and Mesopotamian settlers used a mixture of mud and straw to create strong and durable buildings [2]. Later, in 1200 AD, the Mongols invented the first composite bow using a combination of bamboo, silk, cattle tendons and horns, and pine resin. These bows were extremely powerful and extremely swifter [4].

In the late 1800s, canoe builders began experimenting with different materials to make paper laminates [6]. In 1936, unsaturated polyester resins were patented by Carleton Ellis [7]. Because of their curing properties, they became the primary choice for resins in composites manufacturing. By the late 1930s, other high-performance resin systems had become available, including epoxy resins [8].

In 1907, chemist Leo Hendrik Baekeland created Bakelite, one of the first synthetic resins. The resin was extremely brittle, but it could be softened and strengthened by combining with cellulose [9]. New and better resins were produced during the 1920s and 1930s. In the early 1930s, American Cyanamid and DuPont further developed polymer resins and both companies independently formulated polyester resin for the first time [7].

In the late 1930s, Russell Games Slayter of Owens-Corning developed a process for drawing glass into thin strands or fibers and began weaving them into a textile fabric [10].

Combining these new glass fibers with new synthetic resins to produce strong and lightweight composites. Howard Hughes, an aerospace engineer, used thin wood layers and plastic resin on the Spruce Goose [11].

The newly emerging composites industry further developed during World War II. By 1945, over seven million pounds of fiberglass were used, primarily for military applications [12]. Soon the benefits of FRP (fiber reinforced polymer) composites became known to the public, such as the corrosion resistance. For example, fiberglass pipe was first introduced in 1948 and has become one of its widest areas of use within the corrosion market, the oil industry [13].

Composites continued to grow rapidly through the 1950s and many products were built using composites such as boats, trucks, sports cars, storage tanks, pipes and so on [2]. Since 1981, Chevrolet's Corvette has included transverse composite leaf springs, manufactured by Liteflex [14]. Also in the early 1950s, manufacturing methods such as pultrusion [15], vacuum bag molding [16], and large-scale filament winding [17] were developed.

In 1961, the first carbon fiber was patented. Because of the ability of carbon fiber epoxy composites to withstand extreme conditions, the use of carbon fiber helped advance many applications in a number of industries, including aerospace, automotive, marine and consumer goods [18]. In the mid-1960s, Stephanie Kwolek invented Kevlar [19]. Kevlar is best known for its protective power and thanks to its application in bulletproof vests and body armor, it has saved countless lives.

During the late 1970’s and early 1980’s, composites were first used in infrastructure applications in Europe and Asia. In 1994, the first road lift-bridge in the world was made entirely of advanced composite material [20]. In 1992, a footbridge was built in Aberfeldy, Scotland,

using composite decking sections [2]. The deck structure rails and A-frame towers are made of glass/polyester, and the cables are Kevlar ropes [12].

In the early 2000s, nanotechnology began to be used in commercial products. Carbon nanotubes are used to enhance properties of the bulk products. In the 2010s, with the rise of 3D printing, many composite companies are jumping into the field by 3D printing items with reinforced fibers.

1.4 Manufacturing Methods for Composite Materials

A large number of fabrication methods are in use today. They can be divided into three types: open molding, closed molding and cast polymer molding. Each molding category has a variety of processing methods. They include autoclave, vacuum bag and compression molding, filament winding, fiber placement, injection molding, pultrusion, and resin transfer molding (RTM). A brief description is given below.

1.4.1 Open molding

In open molding, raw materials (resins and fiber reinforcements) are exposed to air as they cure or harden. Open molding utilizes different processes, including hand lay-up, spray-up, casting, and filament winding.

The hand lay-up process is one of the methods that are used currently in different manufactories as fishing boats, automobile and tanks for chemical products because it requires the least amount of equipment. It is a simple and inexpensive process: glass or other reinforcing mat or woven fabric or roving is positioned manually in the mold, and resin is poured, brushed, or sprayed over and into the glass plies [21].

The spray up process is efficient and easily come with design. In this method, resin matrix is sprayed out by the compressed air through the spray gun and at the same time the fiber reinforcement is cut. The sprayed resin will mix with the cut fiber and both of them are sprayed into the mold. The process needs to be repeated to get the designed thickness [22].

In filament winding technique, continuous strand roving is fed through a resin bath and wound onto a rotating mandrel. The roving feed runs on a trolley that travels the length of the mandrel. The filament is laid down in a predetermined geometric pattern to provide maximum strength in the directions required. When sufficient layers have been applied, the laminate is cured on the mandrel. The molded part is then stripped from the mandrel. The filament winding technique is presented in Fig. 1.4.1 [23].

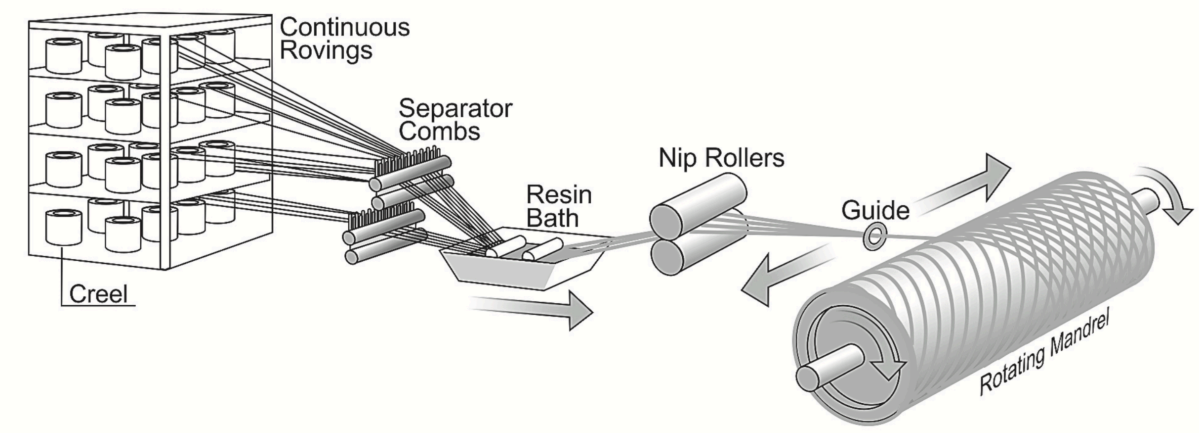

Fig. 1. 2 Schematic presentation of the filament winding technology

1.4.2 Closed molding

In closed-molding, raw materials cure inside a two-sided mold or within a vacuum bag. Closed-molding processes are usually automated and require special equipment, so they're mainly used in large plants that produce huge volumes of material. Closed molding processes include vacuum bag molding, vacuum infusion processing (VIP), resin transfer molding (RTM),

compression molding, pultrusion, reinforced reaction injection molding (RRIM), centrifugal casting and continuous lamination.

Vacuum bag molding improves the mechanical properties of open-mold laminates. By reducing the pressure inside the vacuum bag, external atmospheric pressure exerts force on the bag. The pressure on the laminate removes entrapped air, excess resin, and compacts the laminate, resulting in a higher percentage of fiber reinforcement. An assembly for vacuum bag molding includes a mold for receiving a workpiece. An edge breather comprising a plurality of braided polymer threads is disposed about a periphery of the workpiece. A vacuum bag film is disposed over the workpiece and the edge breather. A seal seals the vacuum bag film to the mold and a passageway in fluidic communication with the edge breather [24]. A schematic is shown in Fig. 1.4.2.1 [25].

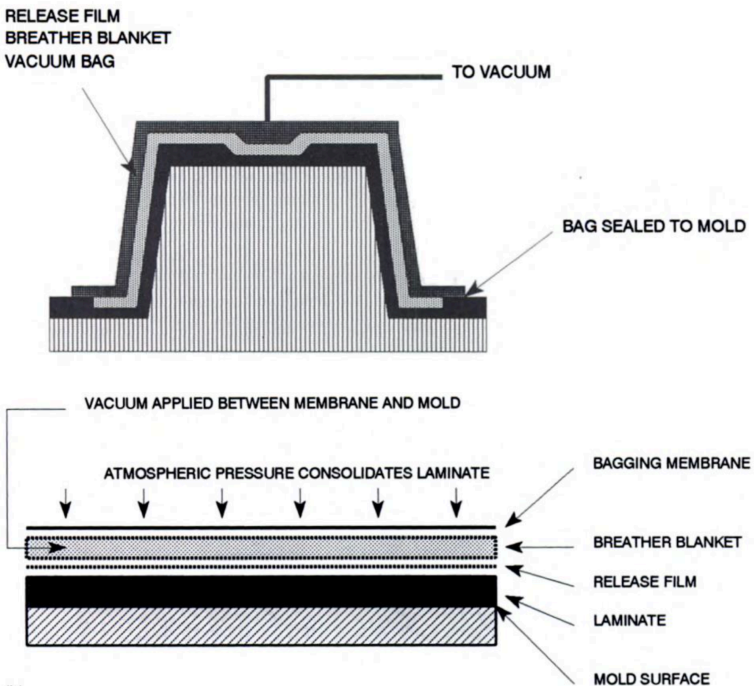

Fig. 1. 3 Vacuum bag molding (a) Schematic (b) The finished laminate is covered with a release film, a porous breather blanket, and then a thin polyamide or rubber bagging film. The applied vacuum evacuates the space between the bag and the tool so that atmospheric pressure acts to consolidate the molding.

Vacuum infusion processing (VIP) is a variation of vacuum bagging in which the resin is introduced into the mold after the vacuum has pulled the bag down and compacted the laminate.

Resin transfer molding (RTM) is an intermediate volume molding process for producing composites. In RTM, resin is injected under pressure into a mold cavity. This process consists of three stages. The first step consists of preparing the fiber reinforcement by cutting and stacking plies of dry fibers, pre-shaping them by heated compaction, and placing them within the mold cavity. The second step involves injecting a pre-catalyzed but uncured thermoset resin into the heated mold cavity and saturating the fibrous preform. The final stage consists of imposing a temperature and pressure cycle that cures the resin while suppressing the formation of microstructural defects [26].

Compression molding is a high-volume, high-pressure method suitable for molding complex, fiberglass-reinforced polymer parts on a rapid cycle time. In compression molding, the raw materials are usually in the form of granules, putty-like masses, or preforms. They are first placed in an open, heated mold cavity. The mold is then closed and pressure is applied to force the material to fill up the cavity. A hydraulic ram is often utilized to produce sufficient force during the molding process. The heat and pressure are maintained until the plastic material is cured.

Pultrusion is a continuous manufacturing process used to produce continuous lengths of reinforced polymer composite materials with constant cross-sections. Raw materials are a liquid resin mixture containing resin, fillers and specialized additives and flexible textile reinforcing fibers. The process involves pulling these raw materials through a heated steel forming die using a continuous pulling device [27].

Reinforced reaction injection molding (RRIM) is a high speed manufacturing process. Two fluid components are mixed to form a thermosetting polymer, injected into a mold under high pressure and then cured [28].

Centrifugal casting is commercially used to produce large diameter composite pipe and tanks. In centrifugal casting, the reinforcement and resin are introduced into a high speed rotating mold. Centrifugal force holds the materials along the mold inner surface until the part is cured [29].

In continuous lamination process, the reinforcement fibers and fabric are impregnated and then guided through pressing rolls. Under elevated temperature and pressure, the desire composite lay-up is cured to have the final dimensions and mechanical properties [30].

1.4.3 Cast polymer molding

Cast polymer molding is used to produce parts of any shape or size. It can be grouped into two general manufacturing methods: gel coated cultured stone molding and solid surface molding.

Gel coat is a specialized polyester resin that can prevent the chalking, whitish discoloration and scratches that can occur over time for composite product. In gel coated cultured stone molding, a gel coat film is sprayed on the mold surface and then a polyester matrix is transferred to the mold after blended with fillers. Pigments can be added to apply color. After the curing process, the part is removed from the mold. Different from the gel coated cultured stone molding, solid surface molding uses vacuum-mixing techniques to produce a matrix that is homogeneous and void free. It is often used to manufacture products like kitchen countertops.

Chapter 2 Experiments

2.1 Materials

The material used in this investigation is 7781 fiberglass pre-preg which is made of fiberglass woven fabrics pre-impregnated with an epoxy resin system. The resin acting as matrix material is a thermoset, capable of being cured from a liquid state to a solid state when subjected to appropriate conditions. Fiberglass woven fabrics are used as the reinforcement with the fibers bundled in two orientations. The warp and fill yarns run at 0 and 90 degrees respectively. Thus, fabrics are anisotropic, or strong in only two directions. Using a pre-preg has both advantages and disadvantages. The greatest advantages is their ease of use, which mean it eliminates the need for hand mixing resin and hardener that is considered hazardous. The disadvantages would be the increased cost due to additional transportation and storage cost. The 7781 fiberglass pre-preg has the fiber aerial weight that is approximately 8.7 ounce per square yard. Resin content is about 42%. The width is 50 inch, Cured ply thickness is 0.010 inch. Table 1 presents the specifications of the material used for the preparation of composite laminates.

Table 2. 1
Specifications of material

Material	Fiber aerial weight ($oz./yd^2$)	Resin content (%)	Width (inch)	Cured ply thickness (inch)
7781 fiberglass pre-preg	8.7	42	50	0.010

2.2 Experiment Methods

Composition, layup sequence and the volume of all laminates were maintained constant for all the trials during the experimentation process. Curing temperature, time and pressure were

selected as the main factors in order to optimize the cure process. In the course of experimentation, two sets of experiments are conducted based on different principles. Preliminary trials confirmed the effect of main parameters selected on the overall quality and strength of the composite laminate and reflect the vague range of each parameter. Additional experiments are conducted based on central composite design to obtain more refined results.

2.2.1 Preliminary Experiments

Temperature, time and pressure were selected as the major factors for the experiments. The factors, their levels and the range selected are presented in Table 2.2. The total number of experimental runs presented by actual values of factors along with the runs is indicated in Table 2.3.

Table 2. 2
Factors and their levels

Factors	Levels						
	1	2	3	4	5	6	7
Temperature (F)	235	250	275	300			
Time (min)	20	30	40	50	60	80	90
Pressure (psi)	0	100	150	200	250	300	320

2.2.2 Central Composite Design (CCD)

Additional experiments were conducted based on central composite design (CCD) approach of design of experiments (DOE). CCD is a powerful experimental technique to study the large number of factors. Two or more factors with three or more levels require increased cost and time of testing. In order to save the same without sacrificing the required quality, CCD method is best suited. Several papers have reported the application of CCD to optimize the manufactory process and properties of the composite materials. Satheesh and Manisekar have used central composite

design method to analyze mechanical properties of nano flyash impregnated GFRP composites [31]. Rostamiyan et al., have employed CCD as an experimental design techniques for the optimization and statistical determination of the significant factor of carbon nanotube influencing on the mechanical properties of Polypropylene [32].

Table 2. 3
Runs and their actual values of factors

Runs	Temperature (F)	Time (min)	Pressure (psi)	Runs	Temperature (F)	Time (min)	Pressure (psi)
1	235	40	200	12	250	50	300
2	235	50	200	13	250	60	0
3	235	50	250	14	275	40	0
4	235	80	100	15	275	40	300
5	235	90	0	16	275	40	350
6	235	90	320	17	275	50	200
7	250	20	200	18	275	50	250
8	250	30	200	19	275	50	300
9	250	50	100	20	300	30	150
10	250	50	200	21	300	40	275
11	250	50	250	22	300	40	300

The ranges and levels of each curing parameter are revised according to the preliminary experiments. The parameters, their levels and the range selected are presented in Table 2.4. The total number of experimental runs presented by both coded and actual values of factors along with the central runs as per CCD approach is indicated in Table 2.5

Table 2. 4
Factors and their levels in CCD experimental plan

Factors		Levels				
		-2	-1	0	+1	+2
Temperature (F)	A	220	235	255	275	290
Time (min)	B	20	40	65	90	110
Pressure (psi)	C	0	50	100	150	200

Table 2. 5
Details of test combinations (tc) in coded and actual values of factor

tc	A	B	C	Temperature in F (A)	Time in min (B)	Pressure in psi (C)
1	-1	-1	-1	235	40	50
2	-1	-1	+1	235	40	150
3	-1	+1	-1	235	90	50
4	-1	+1	+1	235	90	150
5	+1	-1	-1	275	40	50
6	+1	-1	+1	275	40	150
7	+1	+1	-1	275	90	50
8	+1	+1	+1	275	90	150
9	-2	0	0	220	65	100
10	+2	0	0	290	65	100
11	0	-2	0	255	20	100
12	0	+2	0	255	110	100
13	0	0	-2	255	65	0
14	0	0	+2	255	65	200
15	0	0	0	255	65	100
16	0	0	0	255	65	100

2.3 Specimen Preparation

The composite specimens used in this study were manufactured using hand layup techniques. Firstly the pre-preg was cut into smaller pieces with the shape of a rectangle. The length is 5 inches and width is 4 inches. Then, six pieces of pre-preg were stacked one by one to become one laminate. After that the laminate was placed between two release peel plies which act as a releasing agent for easy and quick removal of composite panel. Next the laminate covered with release peel plies was put between two bleeders. As a bleeder, it allows for pressure to be applied uniformly across the entire surface of the laminate. It also absorbs excess resin during the fabrication process. Finally, the bagging film is used on the outside of the bleeder for resisting the high temperature and pressure and prevents the platen being polluted by the resin.

Release peel ply, bleeder and bagging film should be thrown away after use. Fig. 2.1 shows the picture of the manual layup laminate.

Fig. 2. 1 Pre-cure setting of the layup

2.4 Laminating Process

The laminating process of sample was performed manually using Carver Bench Top Standard Heated Model 4128 Press as shown in Fig. 2.2. The machine has two electrically heated steel platens for temperatures up to 650 degree F with digital controller per platen. In this process, the platens were set to the same temperature. Once it reached the pre-set value, the sample in vacuum bagging assembly was placed in the center of the platens. Using the extension handle, the curing pressure can be easily operated and read from the pressure gauge. Once the setting pressure was reach, it was kept constant for specific time. After the curing circle, pressure was unloaded and the finished laminate was cooled down in the room temperature.

Fig. 2. 2 Carver Bench Top Standard Heated Model 4128 Press

2.5 Mechanical property analysis

Flexural modulus (FM) and flexural strength (FS) of the laminates are analyzed in this study. For each type of cured composite laminate, flexural test samples were prepared by cutting the laminate into six flat rectangular specimens, as shown in Fig. 2.3. Three point bending flexural tests were performed on MTS Criterion Model 43 Electromechanical Universal Test System according to ASTM D790 specifications with a 1kN load cell. The crosshead speed was maintained at 0.05mm/s. Flexural strength is based on interfacial strength between the matrix and the fiber. It is helpful in understanding the bonding of the matrix with the fibers. Curing improves the interfacial strength and it is highly relevant to study the flexural strength for determining the optimum cure process parameter. Effective flexural modulus, $\mathbf{E_f}$, was calculated using:

$$\mathbf{E_f} = \frac{\mathbf{mL^3}}{\mathbf{4bd^3}}$$

where m is the slop of initial straight-line portion of three point bending load-deflection curve, L the beam specimen span, b the beam specimen width and d the beam specimen thickness. Flexural strength, $\boldsymbol{\sigma_{fM}}$, was calculated by means of the following equation:

$$\boldsymbol{\sigma_{fM} = \frac{3PL}{2bd^2}}$$

where P is the peak load on the load-deflection curve, L the length of the support span, b the width of beam tested, d the thickness of beam tested.

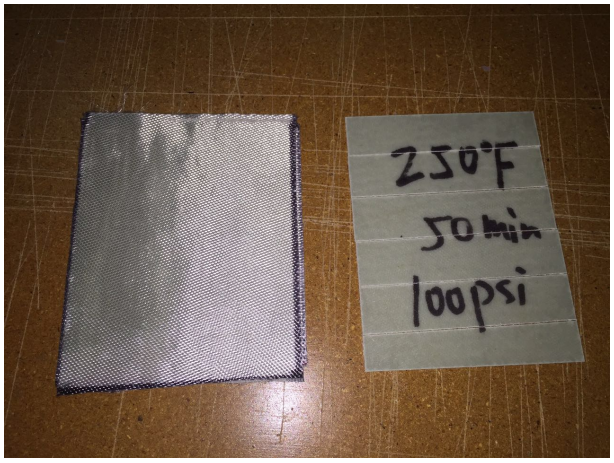

Fig. 2. 3 Flexural test sample

Chapter 3 Results and Discussion

3.1 Experimental Results

In this study, 32 of 34 laminates were carried out three point flexural bending test. There were two laminate lost the results due to computer technical problems. The load-crosshead displacement curves for laminates under different curing parameters are presented as bellow.

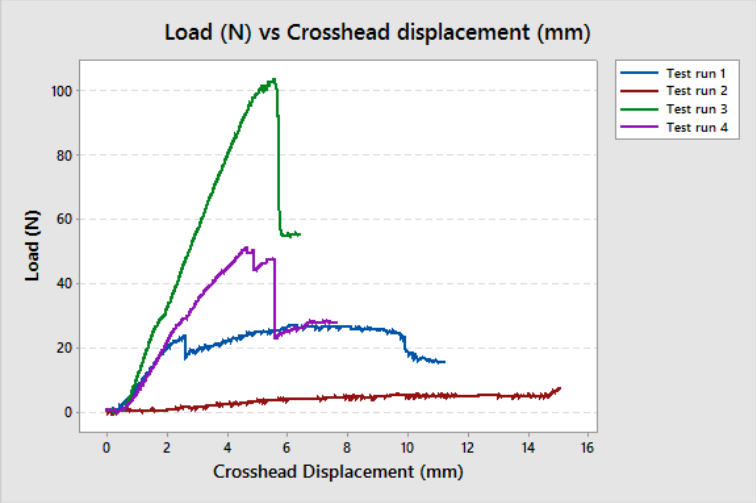

Fig. 3. 1 Load (N) vs. Crosshead displacement (mm) at 235°F, 40min, 200psi

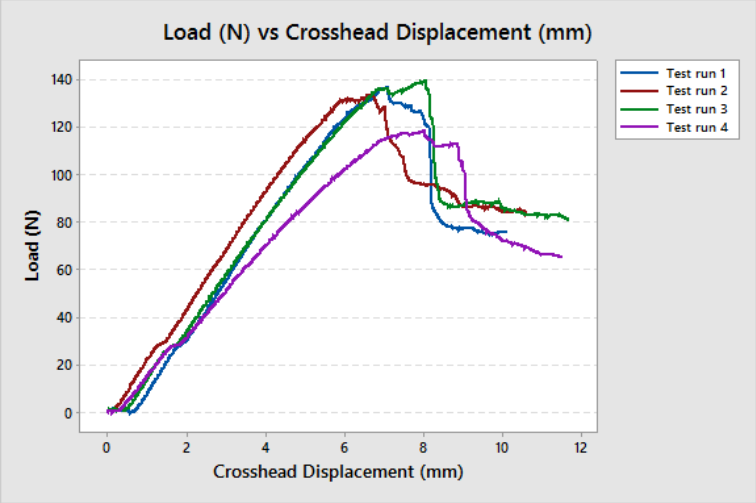

Fig. 3. 2 Load (N) vs. Crosshead displacement (mm) at 235°F, 50min, 200psi

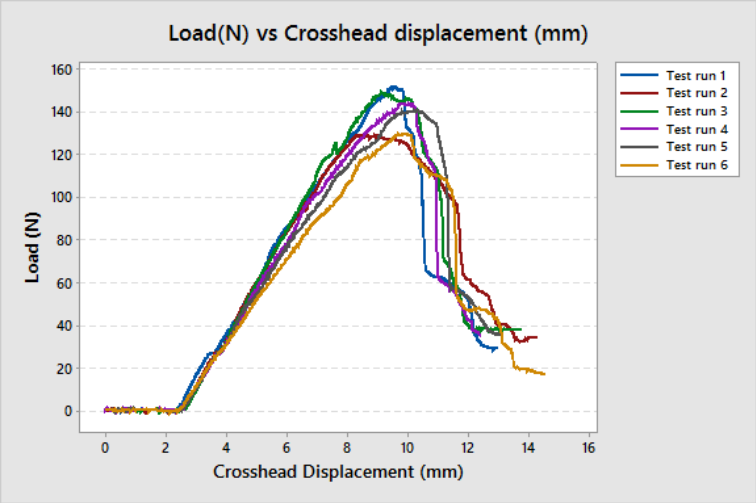

Fig. 3. 3 Load (N) vs. Crosshead displacement (mm) at 235°F, 50min, 250psi

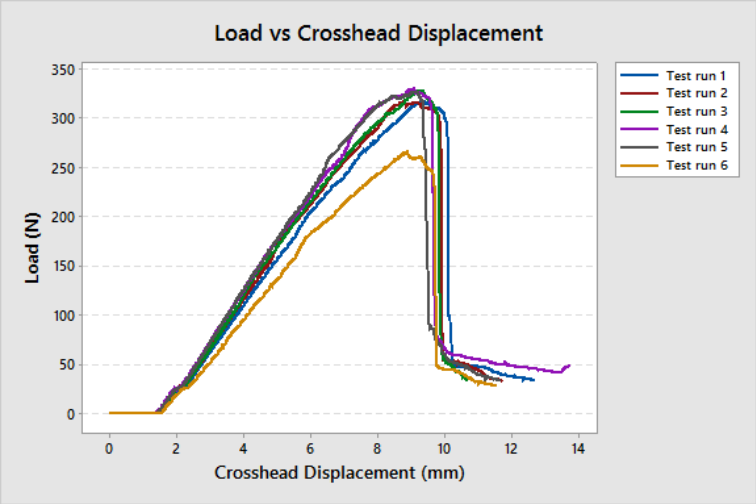

Fig. 3. 4 Load (N) vs. Crosshead displacement (mm) at 235°F, 80min, 100psi

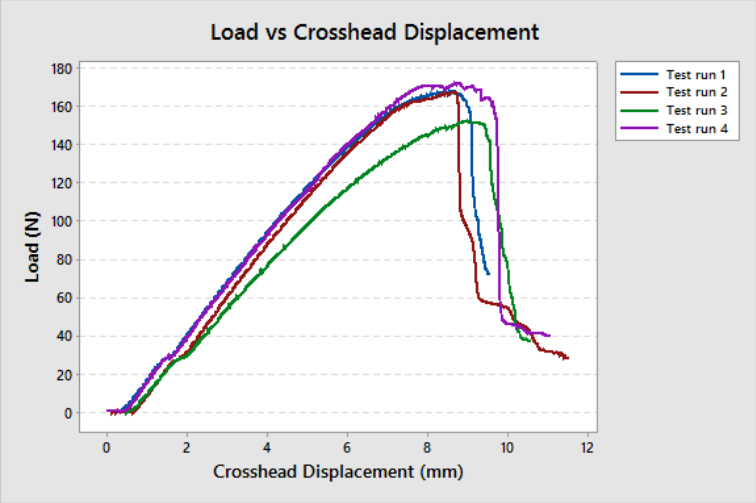

Fig. 3. 5 Load (N) vs. Crosshead displacement (mm) at 235°F, 90min, 320psi

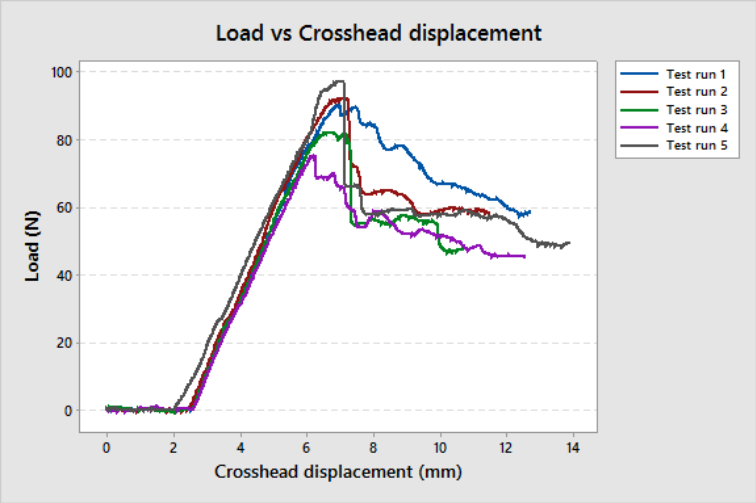

Fig. 3. 6 Load (N) vs. Crosshead displacement (mm) at 250°F, 20min, 200psi

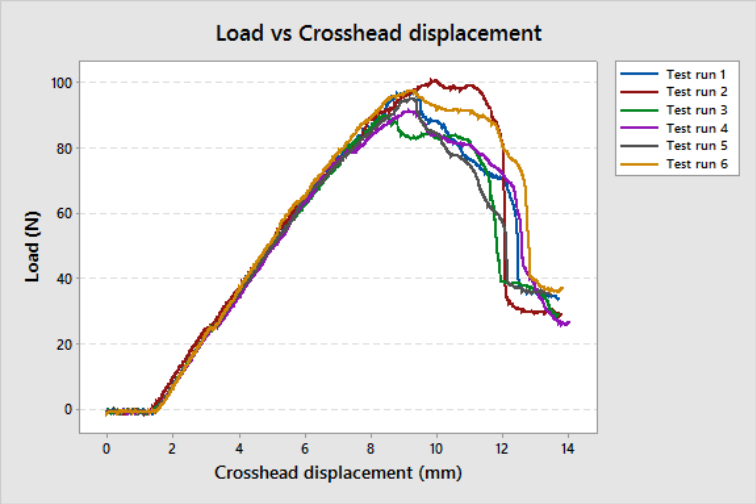

Fig. 3. 7 Load (N) vs. Crosshead displacement (mm) at 250°F, 30min, 200psi

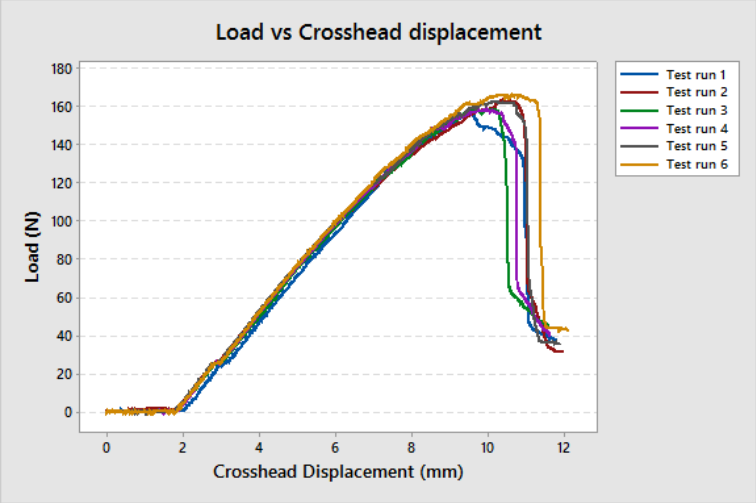

Fig. 3. 8 Load (N) vs. Crosshead displacement (mm) at 250°F, 50min, 200psi

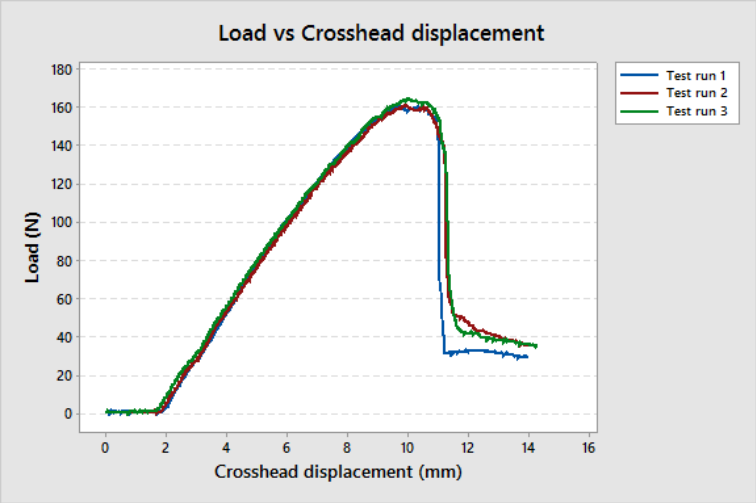

Fig. 3. 9 Load (N) vs. Crosshead displacement (mm) at 250°F, 50min, 250psi

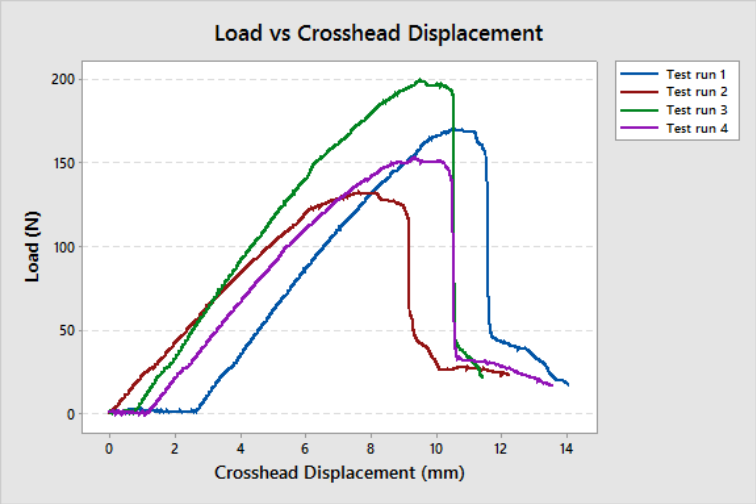

Fig. 3. 10 Load (N) vs. Crosshead displacement (mm) at 250°F, 50min, 300psi

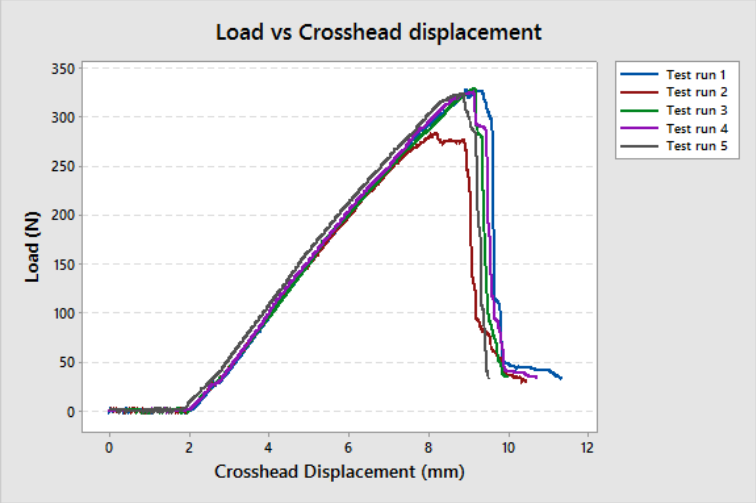

Fig. 3. 11 Load (N) vs. Crosshead displacement (mm) at 275°F, 40min, 0psi

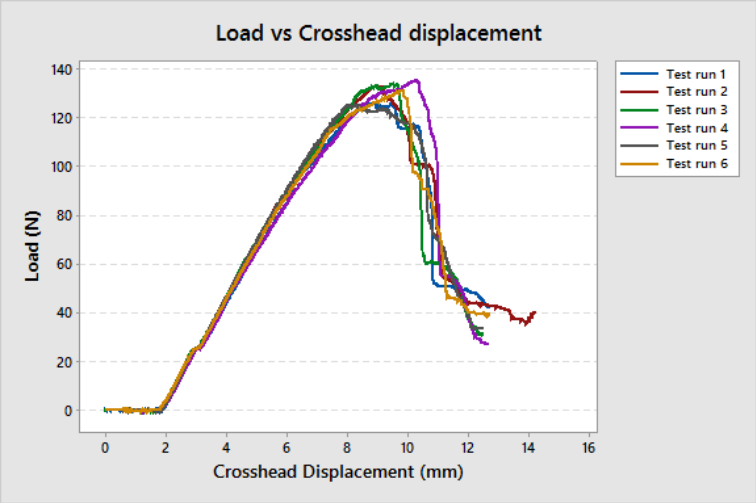

Fig. 3. 12 Load (N) vs. Crosshead displacement (mm) at 275°F, 40min, 300psi

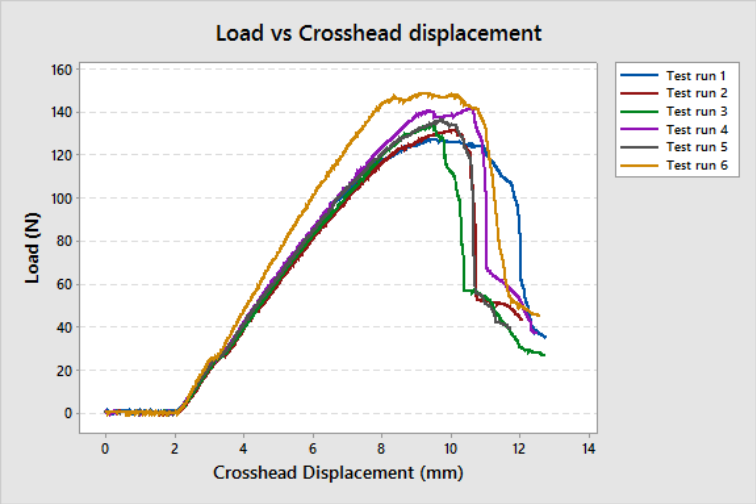

Fig. 3. 13 Load (N) vs. Crosshead displacement (mm) at 275°F, 40min, 350psi

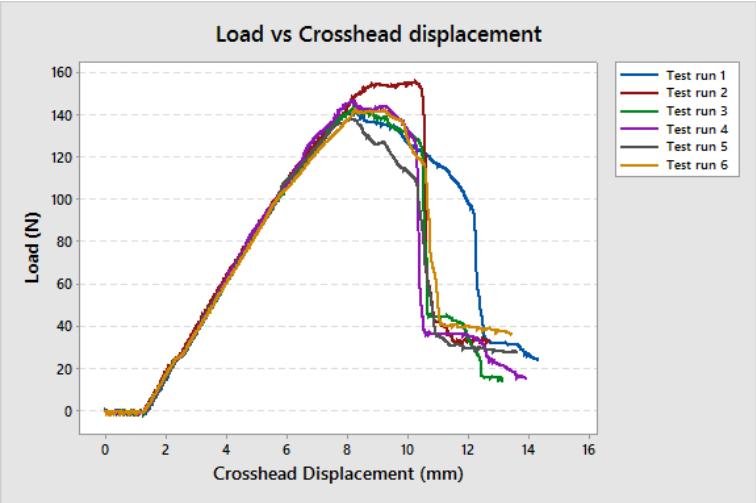

Fig. 3. 14 Load (N) vs. Crosshead displacement (mm) at 275°F, 50min, 200psi

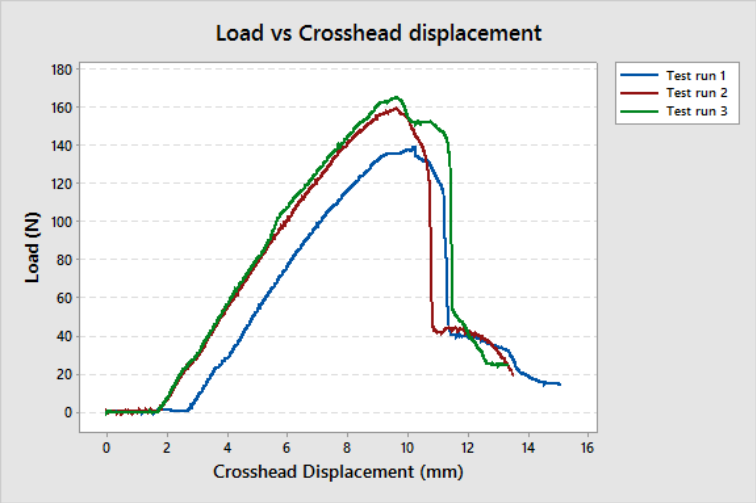

Fig. 3. 15 Load (N) vs. Crosshead displacement (mm) at 275°F, 50min, 250psi

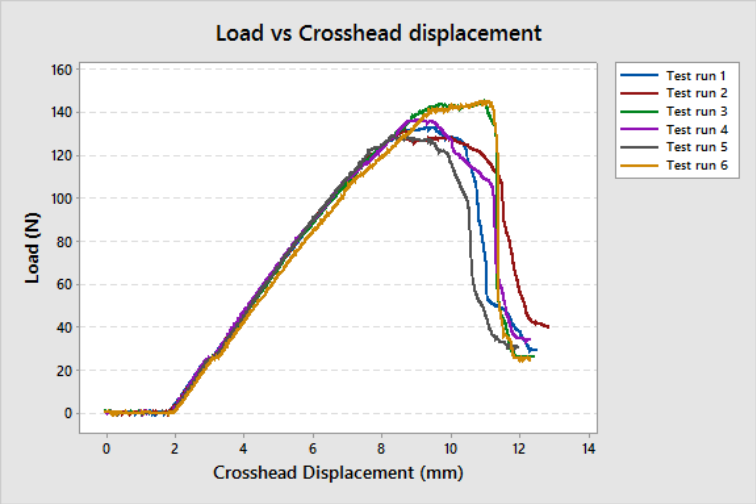

Fig. 3. 16 Load (N) vs. Crosshead displacement (mm) at 275°F, 50min, 300psi

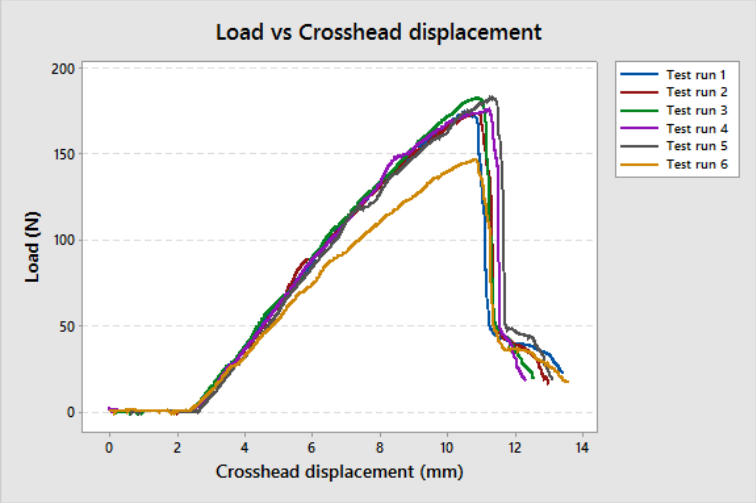

Fig. 3. 17 Load (N) vs. Crosshead displacement (mm) at 300°F, 30min, 150psi

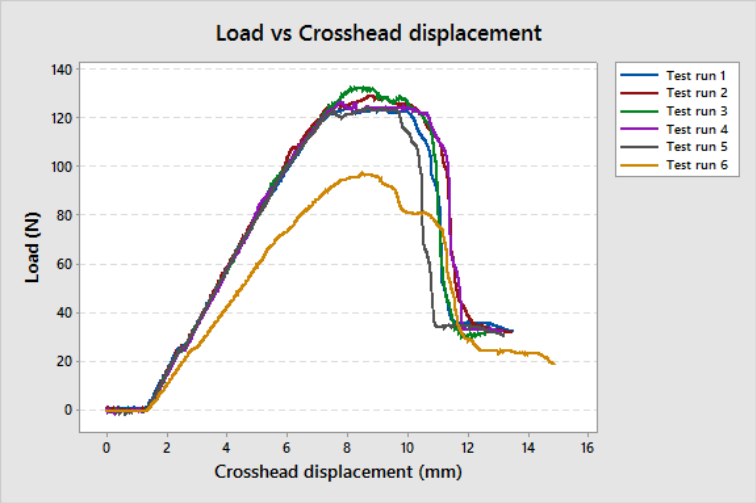

Fig. 3. 18 Load (N) vs. Crosshead displacement (mm) at 300°F, 40min, 300psi

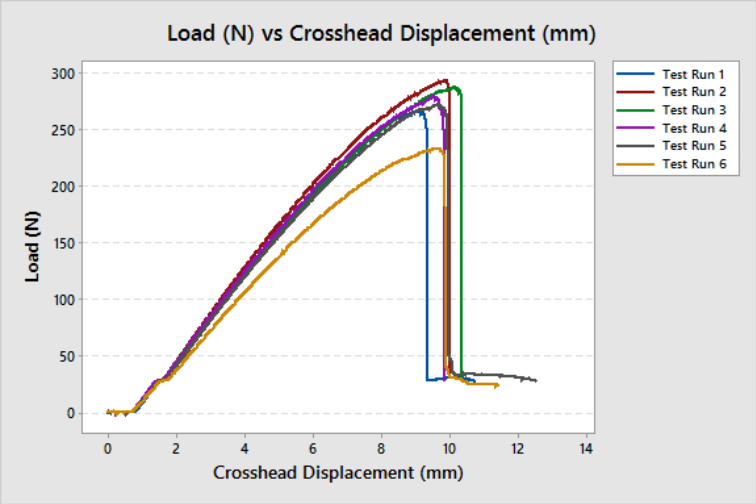

Fig. 3. 19 Load (N) vs. Crosshead displacement (mm) at 235°F, 40min, 50psi

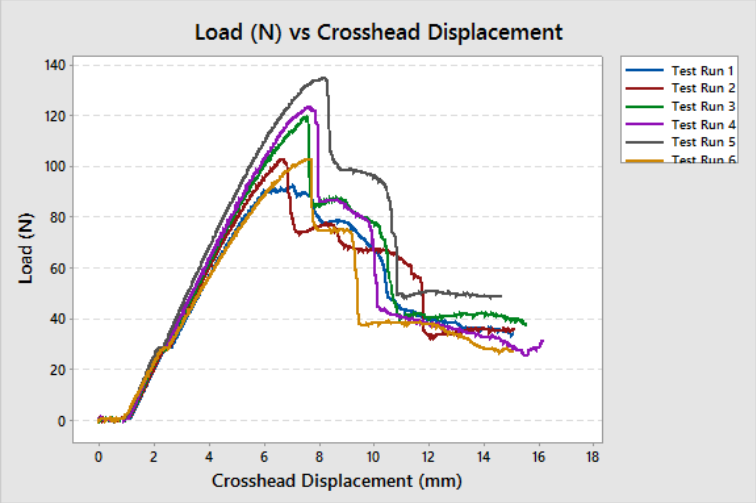

Fig. 3. 20 Load (N) vs. Crosshead displacement (mm) at 235°F, 40min, 150psi

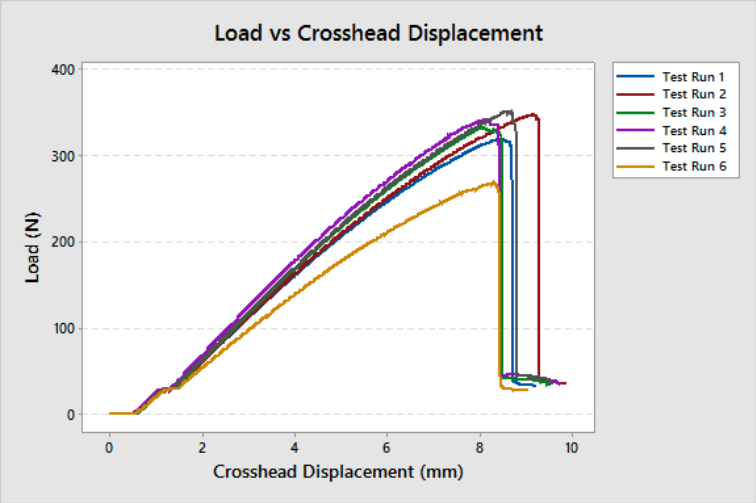

Fig. 3. 21 Load (N) vs. Crosshead displacement (mm) at 235°F, 90min, 50psi

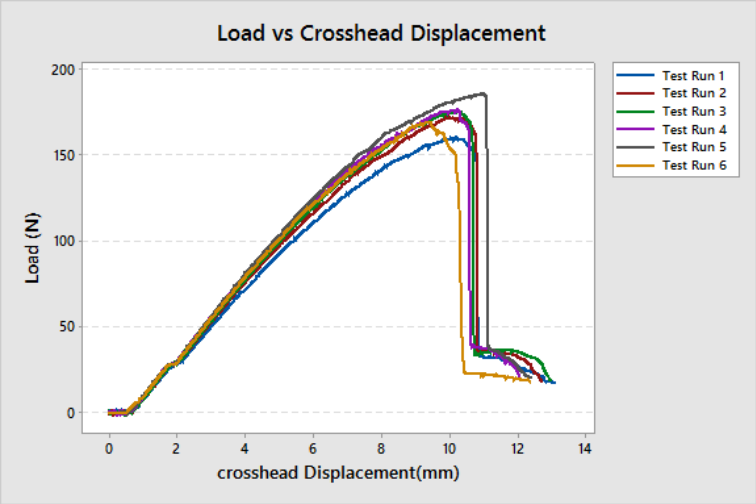

Fig. 3. 22 Load (N) vs. Crosshead displacement (mm) at 235°F, 90min, 150psi

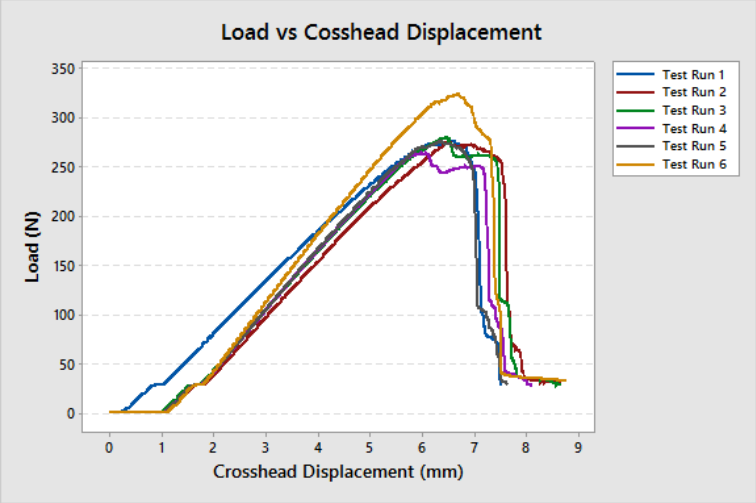

Fig. 3. 23 Load (N) vs. Crosshead displacement (mm) at 275°F, 40min, 50psi

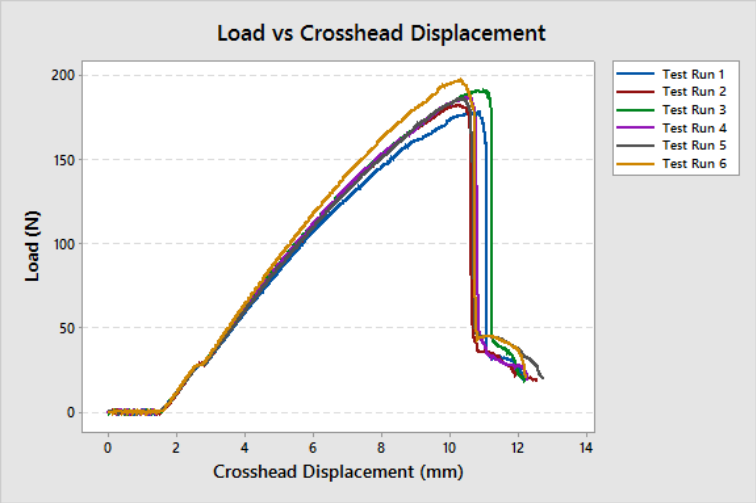

Fig. 3. 24 Load (N) vs. Crosshead displacement (mm) at 275°F, 40min, 150psi

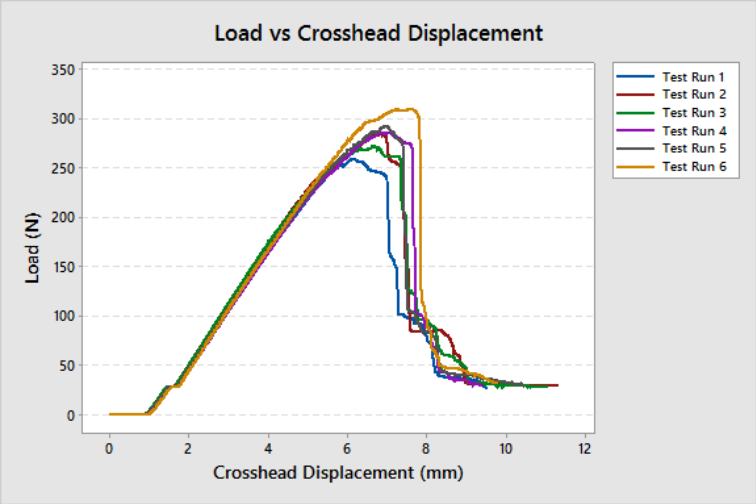

Fig. 3. 25 Load (N) vs. Crosshead displacement (mm) at 275°F, 90min, 50psi

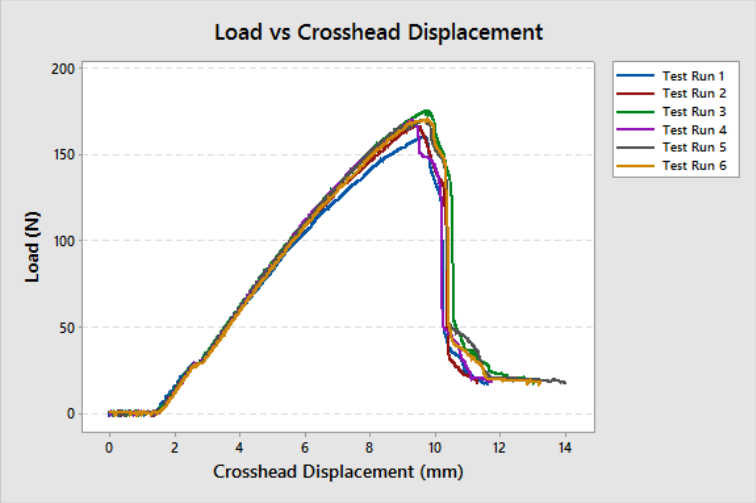

Fig. 3. 26 Load (N) vs. Crosshead displacement (mm) at 275°F, 90min, 150psi

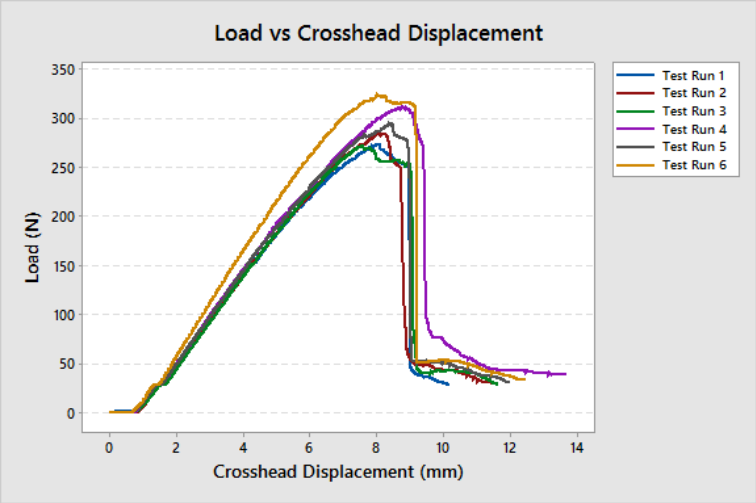

Fig. 3. 27 Load (N) vs. Crosshead displacement (mm) at 220°F, 65min, 100psi

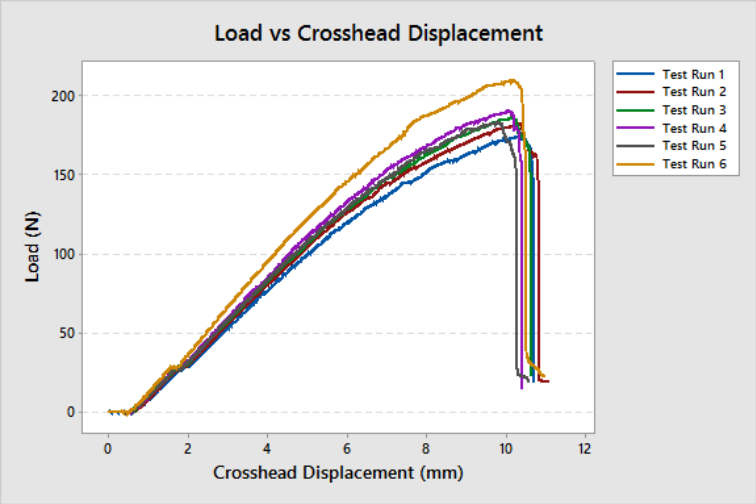

Fig. 3. 28 Load (N) vs. Crosshead displacement (mm) at 290°F, 65min, 100psi

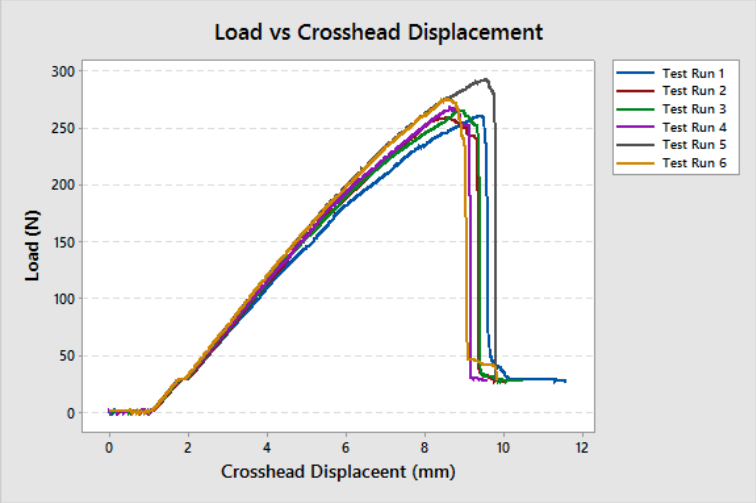

Fig. 3. 29 Load (N) vs. Crosshead displacement (mm) at 255°F, 110min, 100psi

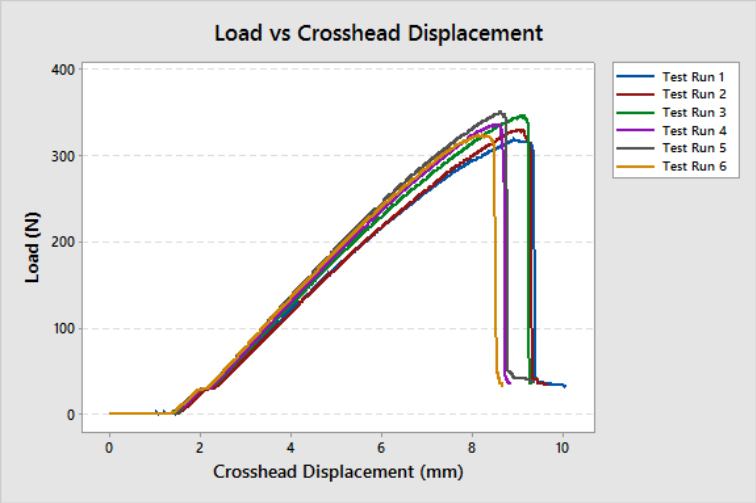

Fig. 3. 30 Load (N) vs. Crosshead displacement (mm) at 255°F, 65min, 0psi

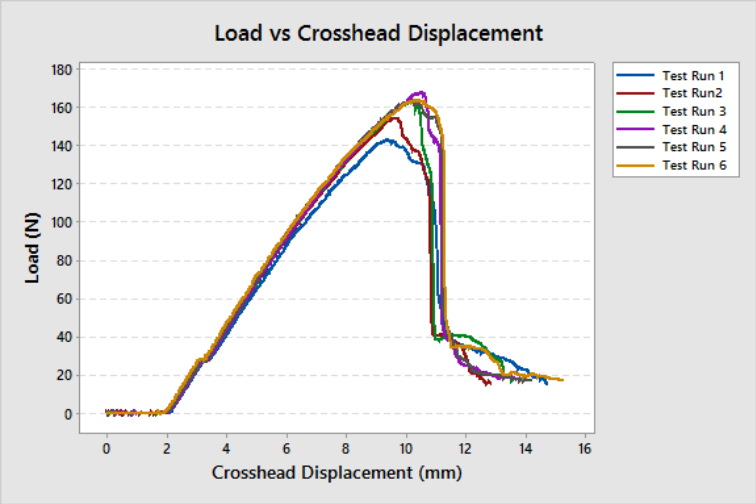

Fig. 3. 31 Load (N) vs. Crosshead displacement (mm) at 255°F, 65min, 200psi

The calculation results of effective flexural modulus and flexural strength according to the flexural tests conducted as per experimental plan is presented in Table 3.1.

Table 3. 1
Results of three point bending tests.

tc	Temperature (°F)	Time (min)	Pressure (psi)	Flexural modulus (GPa)	Flexural strength (MPa)
1	235	40	200	Delamination	
2	235	50	200	16.87675657	293.1476756
3	235	50	250	19.5344228	363.2986314
4	235	80	100	14.5220433	397.1474412
5	235	90	320	19.08159027	382.2580944
6	250	20	200	20.04206287	215.7501669
7	250	30	200	17.96932779	322.0839846
8	250	50	200	16.20254914	366.317806
9	250	50	250	19.92534734	414.3035365
10	250	50	300	20.53679731	419.923369
11	275	40	0	16.08763957	394.8072235
12	275	40	300	18.47412699	335.0462079
13	275	40	350	16.84510113	336.4795694
14	275	50	200	19.97308277	365.3384703
15	275	50	250	19.73122038	388.8888507
16	275	50	300	19.15966905	358.3475515
17	300	30	150	19.04975591	432.6218191
18	300	40	300	21.29043802	347.5305306
19	235	40	50	14.56973702	433.9642465
20	235	40	150	15.10840908	270.5201412
21	235	90	50	14.45696034	427.8398298
22	235	90	150	17.49252314	440.1420191
23	275	40	50	13.68628405	299.1854308
24	275	40	150	17.23300279	428.7342355
25	275	90	50	12.76633267	296.8941864
26	275	90	150	18.49387004	409.9742306
27	220	65	100	14.99695546	393.7707747
28	290	65	100	17.51111875	406.3845778
29	255	110	100	14.88947494	405.9512632
30	255	65	0	14.19901195	400.2019469
31	255	65	200	19.37658945	410.7236072

3.2 Analysis of Results

The experimental results are analyzed with the help of Minitab 17, statistical analysis software, which is widely used in many fields of engineering research. Results are analyzed and modeled by regression analysis which is used to investigate and model the relationship between a response variable and one or more predictors. Response surface and corresponding contour plots give wider insight to understand any problem in general, and to optimize the factors influencing the response in particular. In this study, the number of predictors is large so before fitting a regression model with all the predictors, stepwise model selection technique was used to screen out predictors not associated with the response.

Table 3. 2
Stepwise table for flexural modulus

	Step 1		Step 2		Step 3		Step 4	
	Coef	P	Coef	P	Coef	P	Coef	P
Constant	17.336		17.336		17.887		18.030	
Pressure	1.802	0.000	1.747	0.000	1.728	0.000	1.705	0.000
Temperature			0.484	0.096	0.577	0.040	0.605	0.038
Pressure*Pressure					-0.57	0.043	-0.586	0.035
Time							-0.071	0.811
Time*Pressure							0.494	0.130
S		1.55208		1.50008		1.41097		1.38100
R-sq		58.27%		62.41%		67.97%		71.68%
R-sq(adj)		56.78%		59.63%		64.28%		65.78%
R-sq(pred)		50.65%		52.64%		52.06%		49.74%
Mallows' Cp		5.98		4.81		2.54		3.70

Candidate terms used to stepwise selection are Temperature, Time, Pressure, Temperature*Temperature, Time*Time, Pressure*Pressure, Temperature*Time, Temperature*Pressure, Time*Pressure and Temperature*Time*Pressure. Two-sided confidence interval was used and the confidence level is 95. Predictors were standardized by subtracting the

mean, then divide by the standard deviation in order to center the predictors and to place them on a comparable scale. The output of stepwise model selection is presented in Table 3.2.

This table displays the stepwise model selection results at each step based on the alpha-to-enter value. The table includes the coefficient and p-value for the included predictors. The p-values are used to determine whether the predictor is entered or removed from the model. For the flexural modulus, four steps are used to select the predictors. At the first step, Pressure has the smallest p-value less than the alpha-to-enter value that is equal to 0.15. Therefor, Pressure is the first predictor to e entered into the model. At the second step, Temperature has the smallest p-value less than 0.15, so it is the second predictor to be entered into the model. At the third step, the two-way interaction Pressure*Pressure enters the model. In this model, the coefficient of Pressure*Pressure is -0.57, and the p-value is 0.043. At the forth step, Time and Time*Pressure enters the model. After the forth step, no predictors outside the model have p-values less than 0.15, and no predictors in the model have p-values greater than 0.15. Therefore, no predictors can be entered into or removed from the model. The final model includes five terms: Pressure, Temperature, Pressure*Pressure, Time, and Time*Pressure.

The statistics included in the table are S, R-sq, R-sq (adj), R-sq (pred) and Mallows' Cp. S is measured in the units of the response variable and represents the standard distance that data values fall from the regression line. For a given study, the better the equation predicts the response, the lower S is. R-Sq is the proportion of the variation in the response data explained by the model. The larger the R², the better the model fits the data. R-Sq(adj) is a modified R^2 that has been adjusted for the number of terms in the model. R-sq(pred) is another R^2 like statistic that reflects how well the model predicts future data. Mallows' Cp assesses how well the model

fits the data. Mallows' Cp should be close to the number of predictors contained in the model plus the constant.

Comparing the models at each step, we can see that S decreases from step 1 to step 4, R-sq and R-sq (adj), and R-sq (pred) increase from step 1 to step 4, and Mallows' Cp becomes virtually equal to the number of predictors plus constant in the model. Taken together, these statistics indicate that the step 4 model, containing the terms Pressure, Temperature, Pressure*Pressure, Time, and Time*Pressure, provides a better fit for the data.

Table 3. 3
ANOVA results for flexural modulus, using adjusted SS for tests.

Source	DF	Adj SS	Adj MS	F-Value	P-Value
Regression	5	115.856	23.1712	12.15	0.000
Temperature	1	9.163	9.1634	4.80	0.038
Time	1	0.111	0.1114	0.06	0.811
Pressure	1	77.662	77.6619	40.72	0.000
Pressure*Pressure	1	9.473	9.4728	4.97	0.035
Time*Pressure	1	4.693	4.6926	2.46	0.130
Error	24	45.772	1.9072		
Total	29	161.627			

S=1.38100, R-sq=71.68%, R-sq(adj)= 65.78%, R-sq(pred)= 49.74%

Table 3. 4
Regression analysis for flexural modulus.

Term	Coef	SE Coef	T-Value	P-Value	VIF
Constant	18.030	0.371	48.66	0.000	
Temperature	0.605	0.276	2.19	0.038	1.16
Time	-0.071	0.293	-0.24	0.811	1.30
Pressure	1.705	0.267	6.38	0.000	1.09
Pressure*Pressure	-0.586	0.263	-2.23	0.035	1.03
Time*Pressure	0.494	0.315	1.57	0.130	1.14

ANOVA results of flexural modulus are given in Table 3.3. It can be observed that the Temperature, Pressure, and Pressure*Pressure are significant as the P-value for these is below 0.05. Use the p-values to determine which coefficients in the model are significantly different from zero (no effect). After identification of a significant set of effects, coefficients table is used to evaluate the individual effects. The coefficients table is presents in Table 3.4. It lists the estimated coefficients for each level of each factor. We can see the VIFs are close to 1, which indicates that the predictors are not correlated and well estimated. Thus the regression coefficients are stable and reliable.

Fig. 3.32 shows the variation of each factor and the corresponding flexural modulus response obtained. The flexural modulus increases significantly with respect to pressure, it is 13 GPa under a pressure of 0 psi and goes up to 19 GPa under a pressure of 300 psi, indicating that the pressure has significant effect on the flexural modulus of the laminates. The temperature vs. flexural modulus plots also shows the same phenomena. The response of time to flexural modulus is almost parallel to the x-axis between 20 min to 90 min, then there is no main effect present. Thus resulting in considerable reduction in process curing time. The inference that can be drawn from this plot is, curing pressure and temperature are critical factors.

Fig. 3.33 shows the interaction plot of time and pressure for flexural modulus. In row 1 panel, the lines for the two levels of Time increase as Pressure increases but at different rates. In row 2 panel, the red line (Pressure=350) increases as Time increases, whereas the blue line (Pressure=0) decreases as Time increases. Thus both panels indicate that these two variables interact.

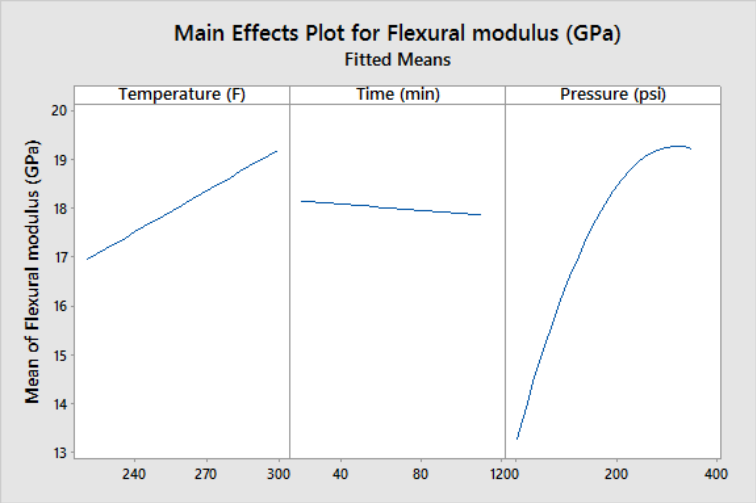

Fig. 3. 32 Main effect plot of factors for flexural modulus.

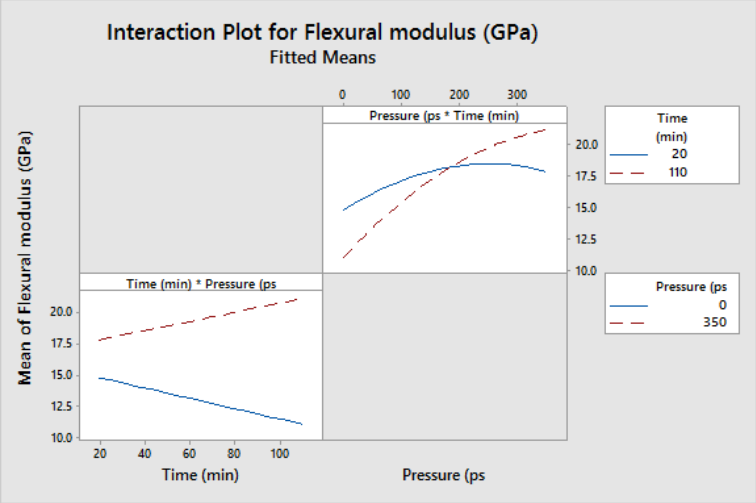

Fig. 3. 33 Interaction plot of time and pressure for flexural modulus.

The regression model in uncoded units is represented by Eq. (3-1), where factors of temperature, pressure and interaction of time and pressure have positive effect. Time and quadratic pressure have negative effect on the overall flexural modulus. The adequacy of the model can be checked by normal probability plot of residuals and the plot of residuals versus fit.

$$\text{Flexural modulus} = 8.38 + 0.0281A - 0.0415B + 0.0252C - 0.000060C*C + 0.000223B*C \quad (3\text{-}1)$$

Where A, B and C are actual values of temperature, time, and pressure.

Fig. 3.34 represents normal probability effect plot of the residuals for flexural modulus. The points lie close to the normality line implying that the errors are distributes normally and the model represented in Eq. (3-1) is adequate. Fig. 3.35 shows the plot of fitted values versus residuals of flexural strength. The points do not form any particular pattern and hence the model represented in Eq. (3-1) is adequate to predict the response.

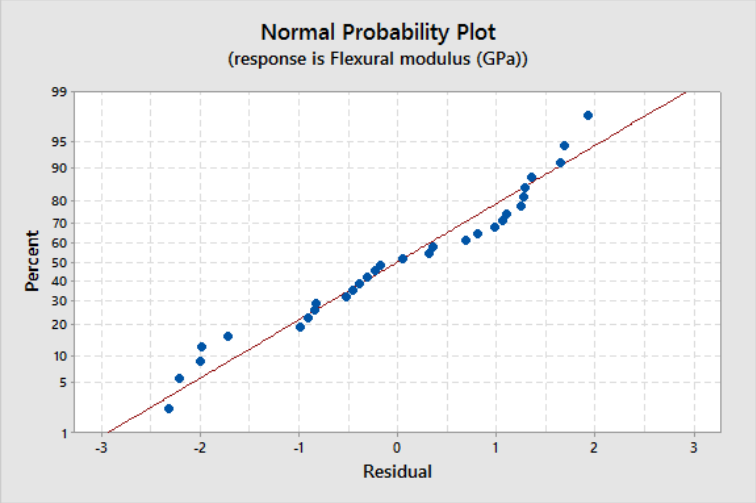

Fig. 3. 34 Normal probability plot of the residuals for flexural modulus.

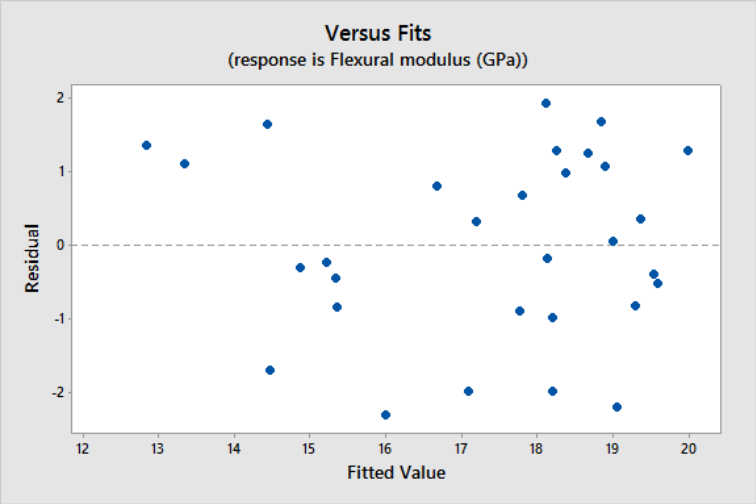

Fig. 3. 35 Plot of residuals vs. the fitted values for the flexural modulus.

Surface plots with flexural modulus as response is plotted for time vs. temperature as shown in Fig. 3.36. The surface plot is a plane surface with rising ridges because of absence of

curvilinear effects of the factors. The optimum points of interest can be obtained and further analysis can be carried out with contour plot for the same as shown in Fig. 3.37. The darkest green area indicates the contour where the flexural modulus is the highest. Since the response surface is a plane and the contour plot contains inclined straight lines. These inclined straight lines in the contour plot of time vs. temperature indicate, only linear effects are present which affect the final strength of the laminate. Temperature of 299 °F and time of 20 min has flexural modulus higher compared to the temperature of 225 °F and time of 95 min as noticed from the plot. As the temperature increases the flexural modulus increases.

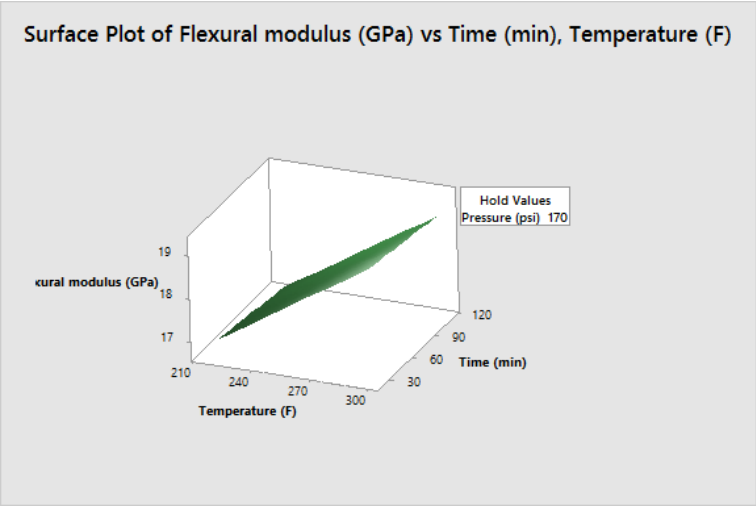

Fig. 3. 36 Surface plot of time vs. temperature for the flexural modulus.

Surface plots with flexural modulus as response is plotted for pressure vs. temperature as shown in Fig. 3.38. The curvilinear surface of the surface plot is due to the presence of interaction effect of pressure and temperature. The curved contour lines present in the contour plot of pressure vs. temperature in Fig. 3.39 are due to interaction effect between these two factors. The optimized region is show in the graph. From Fig. 3.38 the flexural modulus is maximum when temperature is 299 °F and pressure is 349 psi.

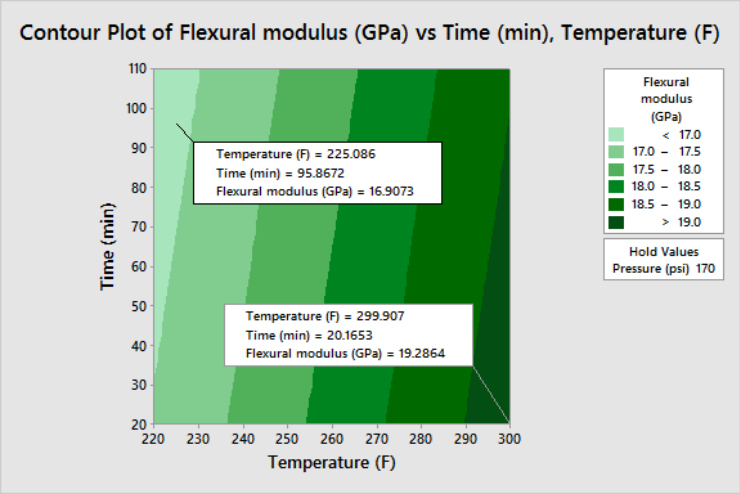

Fig. 3. 37 Contour plot of time vs. temperature for the flexural modulus.

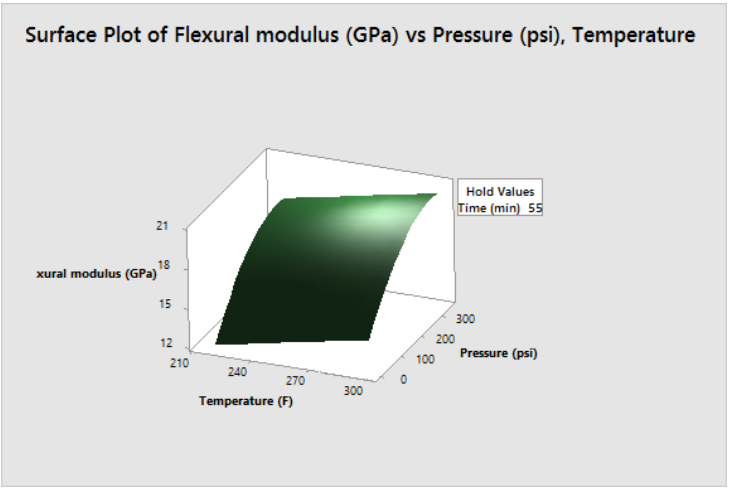

Fig. 3. 38 Surface plot of pressure vs. temperature for the flexural modulus.

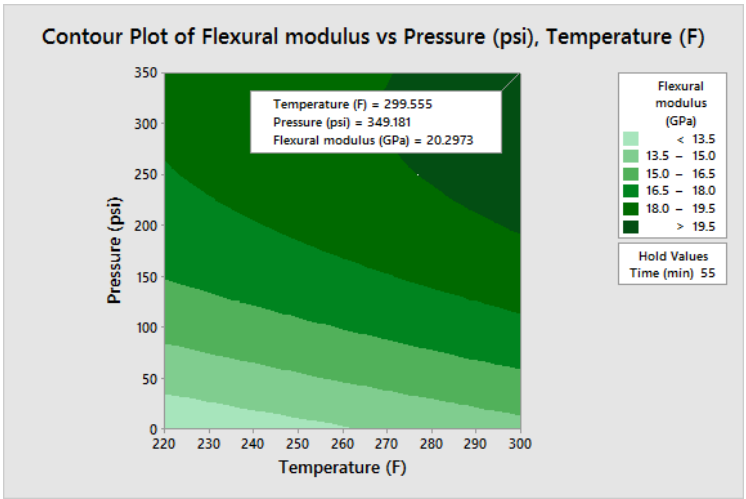

Fig. 3. 39 Contour plot of pressure vs. temperature for the flexural modulus.

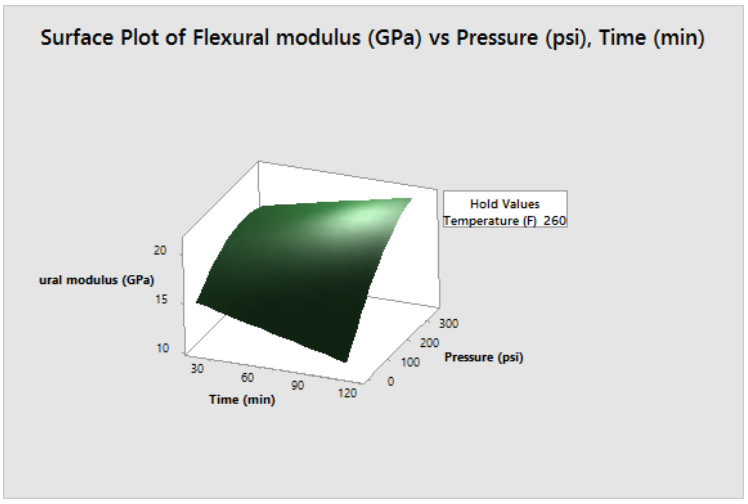

Fig. 3. 40 Surface plot of pressure vs. time for the flexural modulus.

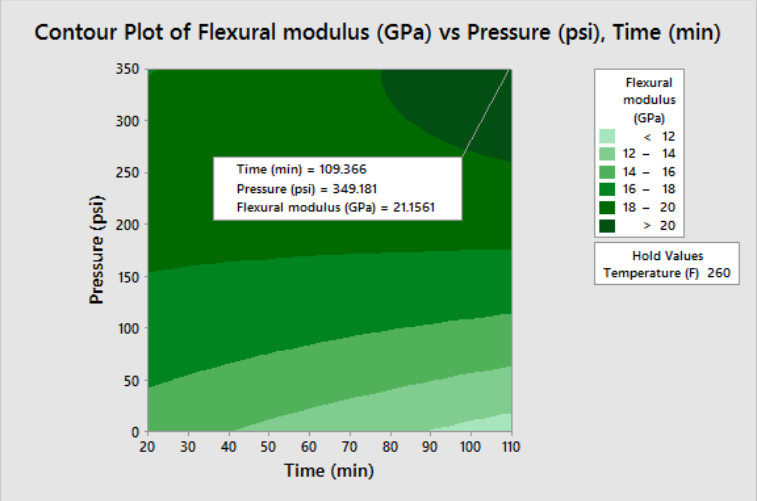

Fig. 3. 41 Contour plot of pressure vs. time for the flexural modulus.

Surface plots with flexural modulus as response is plotted for pressure vs. time as shown in Fig. 3.40. The curvilinear surface of the surface plot is due to the presence of interaction effect of pressure and temperature. The curved contour lines present in the contour plot of pressure vs. time in Fig. 3.41 are due to interaction effect between these two factors. The optimized region is show in the graph. From Fig. 3.38 the flexural modulus is maximum when time is 109 min and pressure is 349 psi.

From Fig. 3.36 to Fig. 3.41, we can see that the temperature and pressure have positive effect on the flexural modulus. However, extending the curing time too much has negative effect on the flexural modulus.

Similar analysis is carried out for the values of flexural strength. Candidate terms used to stepwise selection are Temperature, Time, Pressure, Temperature*Temperature, Time*Time, Pressure*Pressure, Temperature*Time, Temperature*Pressure, Time*Pressure and Temperature*Time*Pressure. Two-sided confidence interval was used and the confidence level is 95. Predictors were standardized by subtracting the mean, then divide by the standard deviation in order to center the predictors and to place them on a comparable scale. The result of stepwise model selection in Table 3.5 shows different significant factors from tensile strength. For the flexural strength, three steps are used to select the predictors. Comparing the models at each step, the final model includes four terms: Time, Temperature, Temperature*Time, and Time*Time provides a better fit for the data.

Table 3. 5
Stepwise table for flexural strength

	Step 1		Step 2		Step 3	
	Coef	P	Coef	P	Coef	P
Constant	371.92		366.28		382.7	
Time	22.02	0.029	20.73	0.042	33.0	0.006
Temperature			3.58	0.714	4.96	0.593
Temperature*Time			-21.5	0.057	-22.7	0.036
Time*Time					-17.35	0.056
S		51.5970		49.5064		46.8602
R-sq		15.86%		28.08%		38.04%
R-sq(adj)		12.86%		19.78%		28.13%
R-sq(pred)		0.47%		0.00%		0.00%
Mallows' Cp		5.90		5.27		3.49

Table 3. 6
ANOVA results for flexural modulus, using adjusted SS for tests.

Source	DF	Adj SS	Adj MS	F-Value	P-Value
Regression	4	33701.9	8425.5	3.84	0.015
Temperature	1	644.9	644.9	0.29	0.593
Time	1	19716.5	19716.5	8.98	0.006
Time*Time	1	8826.2	8826.2	4.02	0.056
Temperature*Time	1	10836.5	10836.5	4.93	0.036
Error	25	54896.9	2195.9		
Total	29	161.627			

S=46.8602, R-sq=38.04%, R-sq(adj)= 28.13%, R-sq(pred)= 28.13%

ANOVA results of flexural strength are given in Table 3.6. It can be observed that the Time and Temperature*Time are significant as the P-value for these is below 0.05. Temperature is insignificant whereas it has the interaction effect with the time. After identification of a significant set of effects, coefficients table is used to evaluate the individual effects. The coefficients table is presents in Table 3.7. It lists the estimated coefficients for each level of each factor. We can see the VIFs are close to 1, which indicates that the predictors are not correlated and well estimated. Thus the regression coefficients are stable and reliable.

Table 3. 7
Regression analysis for flexural strength.

Term	Coef	SE Coef	T-Value	P-Value	VIF
Constant	382.7	12.2	31.49	0.000	
Temperature	4.96	9.16	0.54	0.593	1.11
Time	33.0	11.0	3.00	0.006	1.60
Time*Time	-17.35	8.66	-2.00	0.056	1.48
Temperature*Time	-22.7	10.2	-2.22	0.036	1.04

Fig. 3.42 shows the variation of each significant factor and the corresponding flexural strength response obtained. The flexural strength increases significantly with respect to time, it is below 300 MPa at a time of 20 min and goes up to 400 MPa at a time of 80 psi, however, at a

time higher than 80 min, the flexural strength starts drop down, indicating that the time has significant effect on the flexural strength of the laminates. The temperature vs. flexural strength plots shows that higher temperatures are associated with higher flexural strength than lower temperatures.

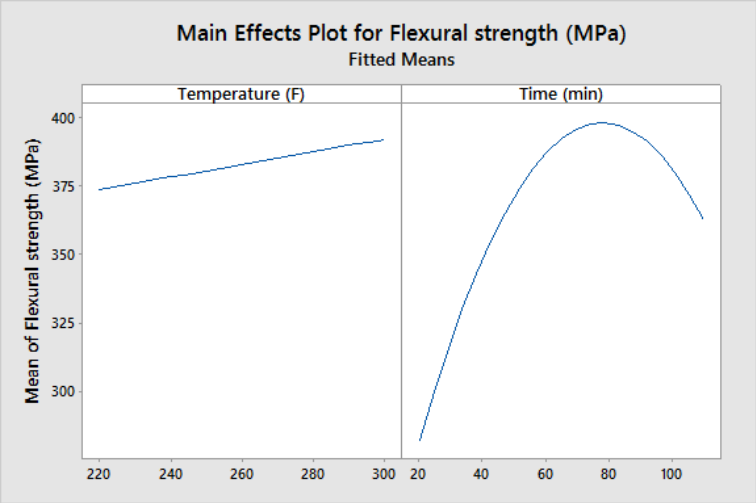

Fig. 3. 42 Main effect plot of factors for flexural strength.

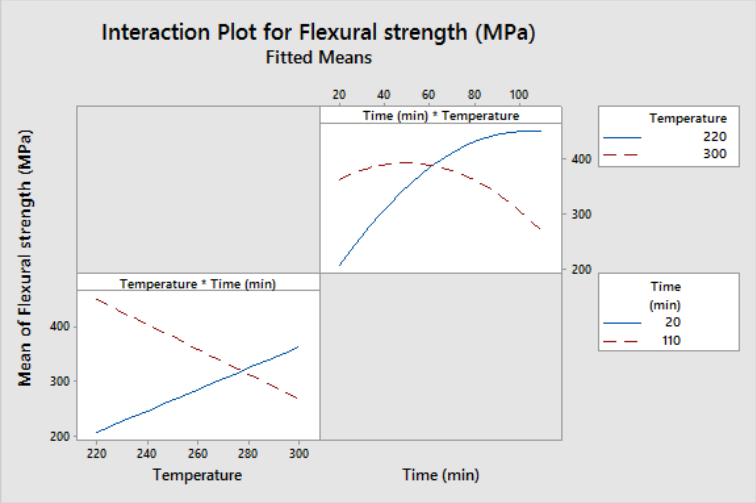

Fig. 3. 43 Interaction plot of temperature and time for flexural strength.

Fig. 3.43 shows the interaction plot of temperature and time for flexural strength. The slopes between the lines are greatly different, indicating the degree of interaction is very high. In row 1 panel, the red line which is at a temperature of 300°F firstly increases, then reaches a

maximum, afterwards decreases as time increases, whereas the blue line which is at a temperature of 220°F keeps increasing as time increases. Two lines cross over at a time of 60 min. In row 2 panel, the red line (Time=110 min) decreases as temperature increases. The blue line (Time=20 min) increases as temperature increases. Two lines intersect with each other at a temperature of 280°F.

Regression analysis was carried out considering the nonlinear effects and there were no nonlinear terms contributing to the flexural strength. Hence only significant factors as indicated in Table 3.7 were included and the mathematical model in uncoded units is represented in Eq. (3-2), where factors temperature and time have positive effect and the interaction of temperature and time has negative effect on the overall strength of the composite. This is quite different from the regression analysis of flexural modulus.

$$\text{Flexural strength} = -559 + 2.89\text{A} + 17.53\text{B} - 0.0345\text{B} * \text{B} - 0.0470\text{A} * \text{B} \quad (3\text{-}2)$$

Where A is actual value of temperature in °F, B is actual value of time in min.

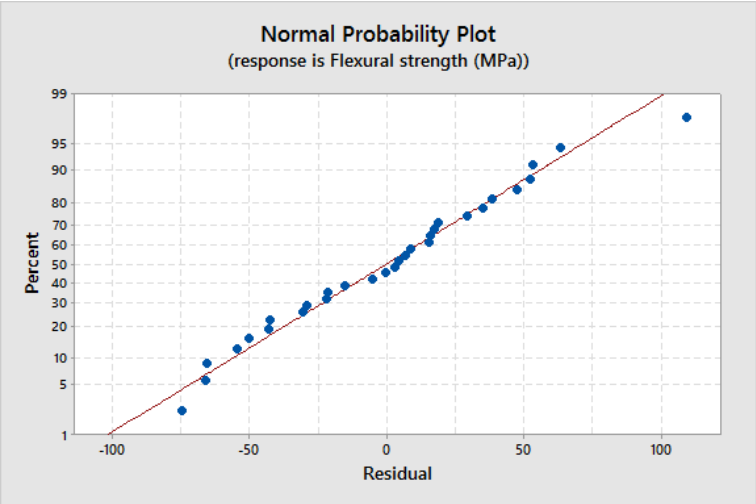

Fig. 3. 44 Normal probability plot of the residuals for flexural strength.

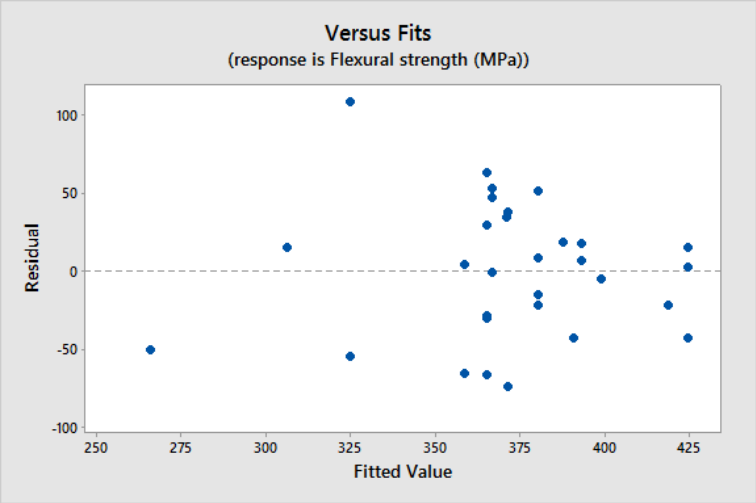

Fig. 3. 45 Plot of residuals vs. the fitted values for the flexural strength

The adequacy of the model can be checked by normal probability plot of residuals and the plot of residuals versus fit. Fig. 3.44 represents normal probability effect plot of the residuals for flexural strength. The points lie close to the normality line implying that the errors are distributes normally and the model represented in Eq. (3-2) is adequate. Fig. 3.45 shows the plot of fitted values versus residuals of flexural strength. The points do not form any particular pattern and hence the model represented in Eq. (3-2) is adequate to predict the response.

Fig. 3.46 and 3.47 respectively show the surface plot and contour plot of flexural strength for time vs. temperature. The surface is a plane with rising ridges. After interpreted the data, we can maximize the strength by setting time near the maximum setting (120 min) and temperature near the minimum setting (210°F). From these settings, strength decreases rapidly if we increase temperature while we hold time constant. Strength also decreases rapidly if we hold temperature constant as we decrease Time. In contour plot, temperature is plotted on the X-axis and time is plotted on the Y-axis. The contour areas represent constant responses, which correspond to strength of 250, 300, 350, 400, and 450. The contour with the darkest green color in the upper left corner indicates the contour where strength is the highest (450). Observe that strength

increases as we move from the lower right to the upper left corner of the plot. That is, strength increases as we simultaneously reduce temperature and increase time. This plot suggests that we can maximize strength at a time more than 110 minutes and a temperature of slightly less than 220°F.

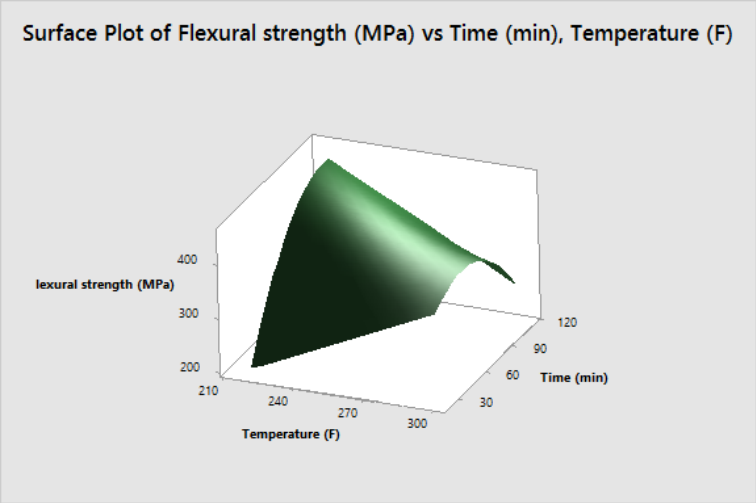

Fig. 3. 46 Surface plot of time vs. temperature for the flexural strength

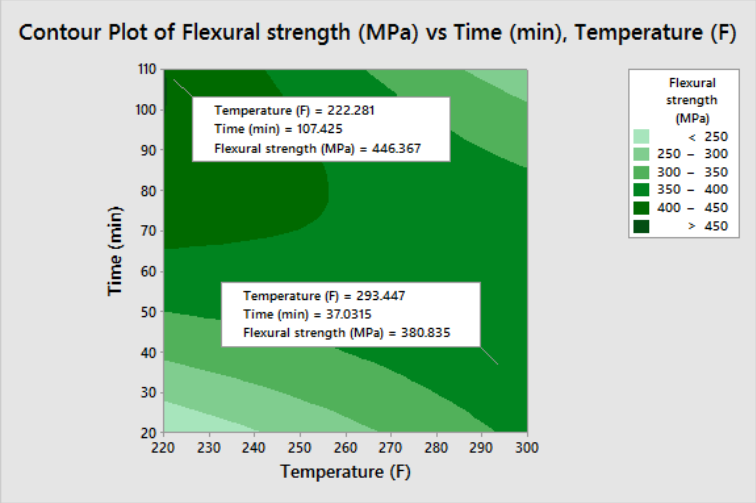

Fig. 3. 47 Contour plot of time vs. temperature for the flexural strength

Overlaid contour plot is shown in Fig. 3.48. It is drawn in order to compare both flexural strength and flexural modulus with respect to significant factors holding the pressure at maximum. Temperature and time are plotted on the X- and Y-axes, respectively. The third

variable, pressure, is held at 350 psi because previous research suggests that higher level of pressure optimizes the flexural modulus. The contours of each response are displayed in a different color. The blue solid contour is the lower bound of flexural strength (250 MPa) while the dotted contour is the upper bound (350MPa). The lower bound of flexural modulus is 18 GPa while the upper bound is 21 GPa. The domain of higher flexural strength and flexural modulus is shown in the plot.

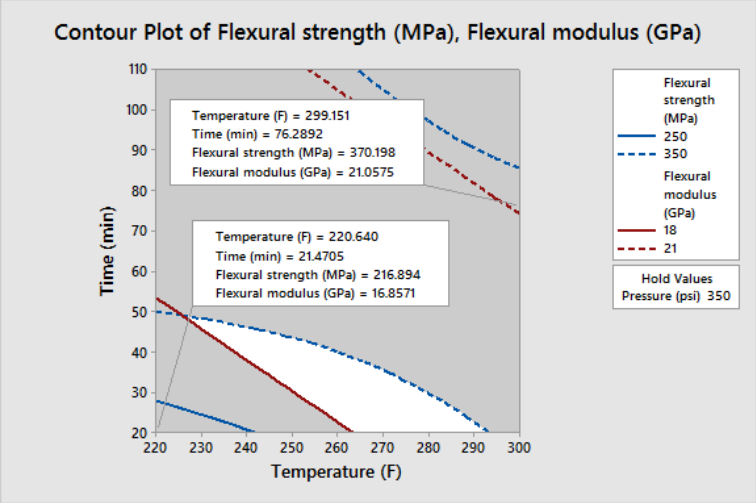

Fig. 3. 48 Overlaid contour plot of flexural strength and flexural modulus.

The optimization plot in Fig. 3.49 shows how the variables temperature, time and pressure affect the flexural strength and flexural modulus and allows us to modify the variable settings interactively. The vertical red lines on the graph represent the current settings. For the experimental data, the current settings are temperature = 300, curing time = 60, and pressure = 321.7172. The horizontal blue lines represent the current response values. The goal was to maximize flexural strength and flexural modulus. Flexural strength has an individual desirability score of 0.778 because the predicted response of 390.3271 is lower than the maximum of 440.142. Flexural modulus has a better desirability score of 0.91122 and the predicted response

is 20.5337. The composite desirability of 0.842 is a good score and indicates that both responses basically achieved their ideal settings.

Table 3.8 shows the prediction based on our models. The Optimized solution is when the parameters at 300°F, 60 min, 321.717 psi.

Table 3. 8
Optimized solution

Response	Fit	SE Fit	95% CI	95% PI
Flexural strength (MPa)	390.3	23.7	(341.5, 439.1)	(282.2, 498.5)
Flexural modulus (GPa)	20.534	0.800	(18.882, 22.185)	(282.2, 498.5)

Temperature=300 °F Time=60 min Pressure=321.717 psi

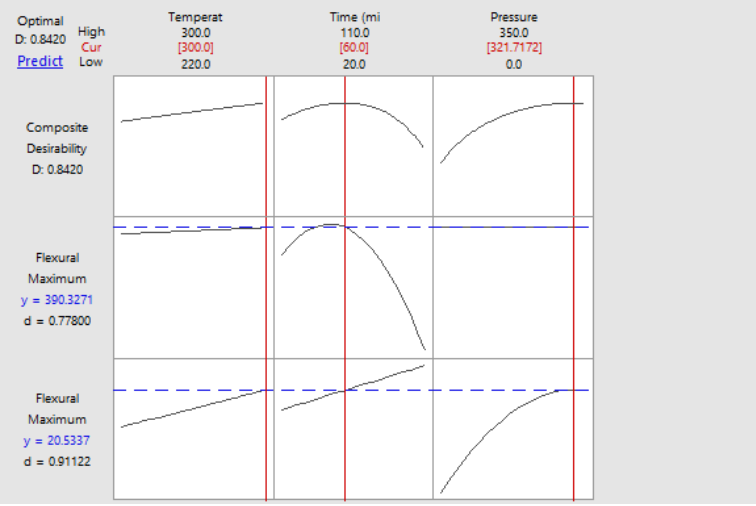

Fig. 3. 49 Optimization plot of flexural strength and flexural modulus

Chapter 4 Conclusions

In this work, the quality of composite laminate in terms of flexural modulus and flexural strength are studied. From the results above, we can see high flexural modulus and high flexural strength can't be obtained at the same time. For flexural modulus, both temperature and pressure have positive effect on it but extending the curing time too much has negative effect. For flexural strength, the interaction between temperature and time has a significant effect on it while the pressure is unimportant. High flexural strength will occurs under long time (above 60 min) and low temperature (below 260 °F) area.

A simple model between layup process parameters and the moduli of the produced composite can be deduced by using regression analysis in Minitab. Flexural modulus=8.38+0.0281A-0.0415B+0.0252C-0.00006C*C+0.000223B*C. Flexural strength=-559+2.89A+17.53B-0.0345B*B-0.0470A*B. By using the models, one can estimate the properties of manufactured composite by knowing the certain processing parameters.

Also, based on the models above, a prediction of optimizing the ideal composite properties was done in Minitab. The Optimized solution is when the parameters at 300°F, 60 min, 321.717 psi. Confirmatory test should be conducted to ascertain the accuracy of prediction in the future.

References

[1] *Structural composites : design and processing technologies : proceedings of the Sixth Annual ASM/ESD Advanced Composites Conference, Detroit, Michigan, USA, 8-11 October 1990*. (1990). Materials Park, Ohio : ASM International, c1990.

[2] Daniel, I. M., & Ishai, O. (1994). *Engineering mechanics of composite materials*. Oxford ; New York : Oxford University Press, c1994.

[3] Nielsen, L. F. (2005). *Composite materials : properties as influenced by phase geometry*. Berlin : Springer, c2005.

[4] Halpin, J. C. (1984). *Primer on composite materials : analysis*. Lancaster, Pa. : Technomic Pub. Co., c1984.

[5] Meikle, J. L. (1995). *American plastic. [electronic resource] : a cultural history*. New Brunswick, N.J. : Rutgers University Press, c1995.

[6] Dawood, E. T. (2015). Experimental study of lightweight concrete used for the production of canoe. *Al-Rafadain Engineering Journal*, *23*(2), 96-106.

[7] Cappitelli, F., & Sorlini, C. (n.d). Microorganisms attack synthetic polymers in items representing our cultural heritage. *Applied And Environmental Microbiology*, *74*(3), 564-569.

[8] LUFT, J. H. (1961). Improvements in epoxy resin embedding methods. *The Journal Of Biophysical And Biochemical Cytology*, *9*409-414

[9] Mercelis, J. (2012). Leo Baekeland's Transatlantic Struggle for Bakelite: Patenting Inside and Outside of America. *Technology And Culture*, (2), 366.

[10] Slayter, G. (1962). TWO-PHASE MATERIALS. *Scientific American*, *206*(1), 124-134.

[11] Thomas, T. (2010). Howard Hughes. *American National Biography (From Oxford University Press)*,

[12] Åström, B. T. (1997). *Manufacturing of polymer composites*. London : Chapman & Hall, 1997

[13] Yagubov, E., Erenkov, O. e., & Radchenko, M. (2013). Study of fiberglass pipe leak-proofness parameters. *Chemical & Petroleum Engineering*, *49*(3/4), 276-280.

[14] Wood, K. (2014). SAVING WEIGHT IN PRODUCTION SUSPENSION SYSTEMS. *Composites Technology*, *19*(1), 34-39.

[15] Shakya, N. S., Roux, J. A., & Jeswani, A. L. (2016). Effect of Fiber Volume Fraction in Fiber Reinforcement Compaction in Resin Injection Pultrusion Process. *Polymers & Polymer Composites*, *24*(1), 7-19.

[16] Lindsay, W. A. (1994). Method for vacuum bag molding fiber reinforced resin matrix composites.

[17] Ansari, S. M., Husin, K., & Ghazali, C. R. (2015). Review on the Application of Natural Fiber Composite via Filament Winding Using Different Resin. *Key Engineering Materials*, *660*120-124. doi:10.4028/www.scientific.net/KEM.660.120

[18] Myers, J. E. (2015). Carbon fiber and carbon nanotubes. *Salem Press Encyclopedia Of Science*,

[19] Rothman, L. (2014, July 7). Stephanie Kwolek. *Time*. p. 21.

[20] Ashley, S. (1995). First plastic bridge. *Mechanical Engineering*, *117*(5), 16.

[21] Belloul, N.)., Hamadache, H.)., Serier, A.)., & Benyahia, A.). (2015). Effect of the aggressive environment on the damage of a glass polyester composite developed by hand layup process. *Advances In Materials Science And Engineering*, *2015*doi:10.1155/2015/207491

[22] Kikuchi, T., Tani, Y., Takai, Y., Goto, A., & Hamada, H. (2014). Mechanical Properties of Jute Composite by Spray up Fabrication Method. *Energy Procedia*, *56*(11th Eco-Energy and Materials Science and Engineering (11th EMSES), 289-297. doi:10.1016/j.egypro.2014.07.160

[23] NASEVA, S., SREBRENKOSKA, V., RISTESKA, S., STEFANOVSKA, M., & SREBRENKOSKA, S. (2015). MECHANICAL PROPERTIES OF FILAMENT WOUND PIPES: EFFECTS OF WINDING ANGLES. *Quality Of Life: A Multi-Disciplinary Journal Of Food Science, Environmental Science & Public Health*, *6*(1-2), 10-15. doi:10.7251/QOL1501010N

[24] VACUUM BAG MOLDING ASSEMBLY AND METHODS. (2014).

[25] *Composites engineering handbook / edited by P. K. Mallick*. (1997). New York: Marcel Dekker, Inc.

[26] Anders, M., Lo, J., Centea, T., & Nutt, S. (2016). Eliminating volatile-induced surface porosity during resin transfer molding of a benzoxazine/epoxy blend. *Composites: Part A, Applied Science & Manufacturing*, *84*442-454. doi:10.1016/j.compositesa.2016.02.024

[27] Carlone, P., Baran, I., Akkerman, R., & Palazzo, G. S. (2015). Computational analysis of the interaction between impregnation, forming and curing in pultrusion. *Key Engineering Materials*, *651-653*889-894. doi:10.4028/www.scientific.net/KEM.651-653.889

[28] Kim, D., & Macosko, C. (n.d). Reaction injection molding process of glass fiber reinforced polyurethane composites. *Polymer Engineering And Science*, *40*(10), 2205-2216.

[29] Vahdat, S. (2016). Tin-Copper-Lead Alloy Produced by Horizontal Centrifugal Casting. *Archives Of Foundry Engineering*, *16*(1), 131-137.

[30] Takechi, K.)., Yamaguchi, S.)., Tanabe, H.)., & Kaneko, S.). (2010). Development of rollable silicon thin-film-transistor backplanes utilizing a roll-to-roll continuous lamination process. *Journal Of The Society For Information Display*, *18*(6), 391-398. doi:10.1889/JSID18.6.391

[31] Satheesh Raja, R., & Manisekar, K. (2016). Experimental and statistical analysis on mechanical properties of nano flyash impregnated GFRP composites using central composite design method. *Materials & Design*, *89*884-892. doi:10.1016/j.matdes.2015.10.043

[32] Y., R., A., F., Abdollah, O., D., G., N., K., & Vahid, S. (2013). Experimental and Statistical Study of Nonlinear Effect of Carbon Nanotube on Mechanical Properties of Polypropylene Composites.